

How does $\text{Mg}^{2+}_{(\text{aq})}$ interact with $\text{ATP}_{(\text{aq})}$? Observations through the lens of liquid-jet photoelectron spectroscopy

Karen Mudryk^{1,‡}, Chin Lee^{1,2,3,†,‡}, Lukáš Tomaník^{4,‡}, Sebastian Malerz¹, Florian Trinter^{1,5}, Uwe Hergenahn¹, Daniel M. Neumark^{2,3}, Petr Slavíček⁴, Stephen Bradforth,^{6*} and Bernd Winter^{1*}

¹Molecular Physics, Fritz-Haber-Institut der Max-Planck-Gesellschaft, Faradayweg 4-6, 14195 Berlin, Germany

²Department of Chemistry, University of California, Berkeley, CA 94720, USA

³Chemical Sciences Division, Lawrence Berkeley National Laboratory, Berkeley, CA 94720, USA

⁴Department of Physical Chemistry, University of Chemistry and Technology, Prague, Technická 5, Prague 6 16628, Czech Republic

⁵Institut für Kernphysik, Goethe-Universität, Max-von-Laue-Straße 1, 60438 Frankfurt am Main, Germany

⁶Department of Chemistry, University of Southern California, Los Angeles, CA 90089, USA

KEYWORDS. *ATP, ICD, Liquid-Jet Photoelectron Spectroscopy, Mg-ATP Interactions, Phosphate Chain*

ABSTRACT: Site-specific information on how adenosine triphosphate in the aqueous phase ($\text{ATP}_{(\text{aq})}$) interacts with magnesium ($\text{Mg}^{2+}_{(\text{aq})}$) is a prerequisite to understanding its complex biochemistry. To gather such information, we apply liquid-jet photoelectron spectroscopy (LJ-PES) assisted by electronic-structure calculations to study $\text{ATP}_{(\text{aq})}$ solutions with and without dissolved Mg^{2+} . Valence photoemission data reveal spectral changes in the phosphate and adenine features of $\text{ATP}_{(\text{aq})}$ due to interactions with the divalent cation. Chemical shifts in Mg 2p, Mg 2s, P 2p, and P 2s core-level spectra as a function of the $\text{Mg}^{2+}/\text{ATP}$ concentration ratio are correlated to the formation of $[\text{MgATP}]^{2-}_{(\text{aq})}$ and $\text{Mg}_2\text{ATP}_{(\text{aq})}$ complexes, demonstrating the element-sensitivity of the technique to Mg^{2+} -phosphate interactions. In addition, we report and compare P 2s data from $\text{ATP}_{(\text{aq})}$ and adenosine mono- and di-phosphate ($\text{AMP}_{(\text{aq})}$ and $\text{ADP}_{(\text{aq})}$, respectively) solutions, probing the electronic structure of the phosphate chain and the local environment of individual phosphate units in $\text{ATP}_{(\text{aq})}$. Finally, we have recorded intermolecular Coulombic decay (ICD) spectra initiated by ionization of Mg 1s electrons to probe ligand exchange in the Mg^{2+} - $\text{ATP}_{(\text{aq})}$ coordination environment, demonstrating the unique capabilities of ICD for revealing structural information. Our results provide an overview of the electronic structure of $\text{ATP}_{(\text{aq})}$ and Mg^{2+} - $\text{ATP}_{(\text{aq})}$ moieties relevant to phosphorylation and dephosphorylation reactions that are central to bioenergetics in living organisms.

INTRODUCTION

The adenosine triphosphate nucleotide in aqueous solution ($\text{ATP}_{(\text{aq})}$) is a complex molecule that enables energy exchange and signal transduction in living organisms.[1-6] It consists of a nucleoside (adenosine, which is formed by adenine and ribose) bound to a chain of three phosphate groups.[7] The biological function of $\text{ATP}_{(\text{aq})}$ stems from dephosphorylation – *i.e.*, liberation of phosphate units – and phosphorylation – *i.e.*, addition of phosphate units – reactions in the aqueous environment of the cell. [8] In the former case, energy is released *via* hydrolysis to produce adenosine diphosphate ($\text{ADP}_{(\text{aq})}$). In the latter case, phosphorylation of $\text{ADP}_{(\text{aq})}$ takes place to restore $\text{ATP}_{(\text{aq})}$ in the cell. Overall, metabolic pathways involving $\text{ATP}_{(\text{aq})}$ and $\text{ADP}_{(\text{aq})}$ are regulated by chemical bond breaking and bond formation at the phosphate chain.[9] While the aforementioned reactions take place either catalyzed by enzymes or non-enzymatically,

the processes are largely determined by the presence of divalent metal cations – such as $\text{Mg}^{2+}_{(\text{aq})}$, the divalent cation with the highest $\text{ATP}_{(\text{aq})}$ binding affinity[10, 11] – and hydration effects inherent to the aqueous environment of the cell.[12-15] In that way, aqueous-phase metal–ligand coordination at the phosphate chain is involved in dephosphorylation (hydrolysis) or phosphorylation at specific phosphate units *via* charge redistribution and conformational changes.[14, 16] On the other hand, nucleic base–metal-ion interactions have been hypothesized, more than half a century ago,[17] to play a role in the overall reaction. A large amount of association equilibria data has been determined in support of such effects.[18] However, the characterization of associated structures by advanced spectroscopic methods is lacking.

The molecular structure of $\text{ATP}_{(\text{aq})}$ is illustrated in Figure 1(a), highlighting the adenine, ribose, and phosphate units. The latter are designated as α , β , and γ (where α refers to the phosphate directly bound to the nucleoside, β refers

to the bridging phosphate unit, and γ refers to the terminal phosphate) and are shown in their deprotonated form

($\text{ATP}^{4-}_{(\text{aq})}$), as predominantly found at physiological pH conditions.[19] We also include the $\text{Mg}^{2+}_{(\text{aq})}$ ion –

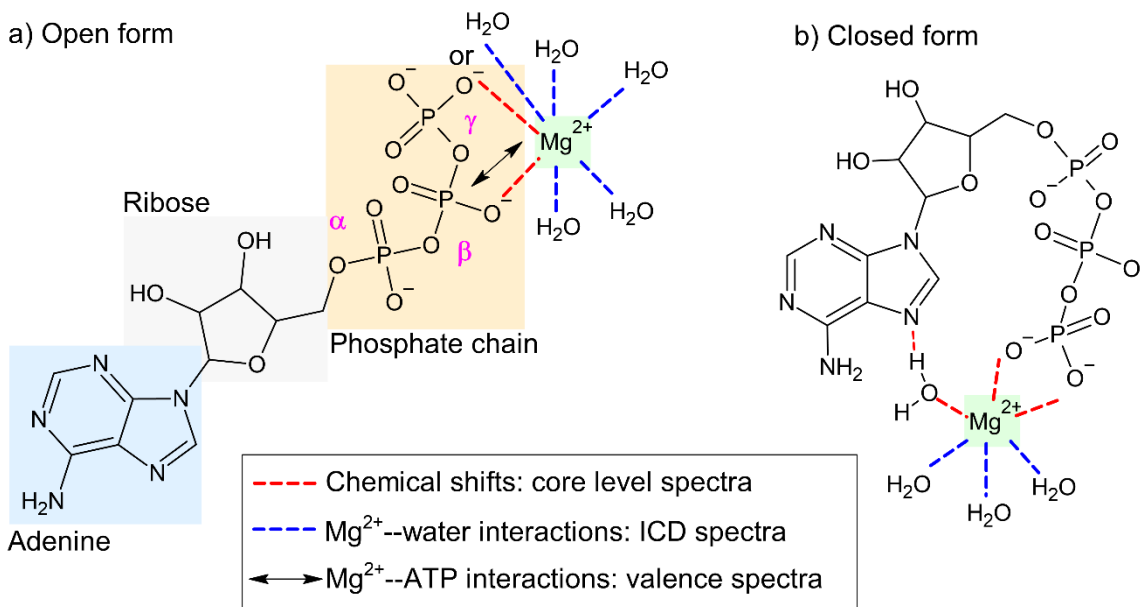


Figure 1. (a) Molecular structure of $\text{ATP}_{(\text{aq})}$ in the deprotonated form ($\text{ATP}^{4-}_{(\text{aq})}$) predominantly found at physiological pH.[19] Adenine, ribose, and α -, β -, and γ -phosphate units are labeled; one of many motifs for Mg^{2+} binding is shown (see text). Binding of $\text{Mg}^{2+}_{(\text{aq})}$ to one *versus* two phosphate units is illustrated by the different interaction strengths (indicated by different lengths of red and blue dashed lines). (b) $[\text{MgATP}]^{2-}_{(\text{aq})}$ complex tentative closed-form structure in which the divalent cation interacts both with an O atom from the phosphate chain and an N atom from the adenine unit in $\text{ATP}_{(\text{aq})}$, with the latter interaction being mediated by a water molecule.[11] Mg^{2+} - $\text{ATP}_{(\text{aq})}$ (probed in valence PE spectra) and Mg^{2+} -water (probed in ICD spectra) interactions are highlighted by red and blue dashed lines, respectively. P- and Mg-specific chemical shifts (probed in core-level PE spectra) are highlighted by a double arrow. Similar structures associated with the $\text{Mg}_2\text{ATP}_{(\text{aq})}$ complex are shown in Figure S1 in the Supporting Information. This figure was produced using the ACD / ChemSketch software.[20] In both cases, the phosphate unit/s interacting with $\text{Mg}^{2+}_{(\text{aq})}$ were chosen arbitrarily.

or more specifically, $[\text{Mg}(\text{H}_2\text{O})_6]^{2+}_{(\text{aq})}$, the octahedral complex configuration adopted by the free ion in aqueous solution [21] – interacting with one or more phosphate units to form various Mg^{2+} - $\text{ATP}_{(\text{aq})}$ complexes,[10, 16] such as $[\text{Mg}(\text{ATP})_2]^{6-}_{(\text{aq})}$,[16, 22-25] $\text{Mg}_2\text{ATP}_{(\text{aq})}$,[26] and $[\text{Mg}_2(\text{ATP})_2]^{4-}_{(\text{aq})}$. [16, 27] In addition to the open form of Figure 1(a), we present in Figure 1(b) a proposed closed form. Here, the metal ion interacts not only with O atoms from the phosphate units (Figure 1(a)), but also, presumably through a water molecule, with an N atom from the adenine unit (Figure 1(b)).[6, 11, 28, 29] The ‘closed form’ / ‘open form’ ratio in aqueous solution has been reported to be 1:10.[11, 28, 30]

Despite a single phosphate unit seemingly being involved in phosphorylation and dephosphorylation reactions,[31] $\text{Mg}^{2+}_{(\text{aq})}$ complexation to multiple sites in the phosphate chain is required for the overall reaction to proceed.[32-35] In the absence of enzymes, α -, β -, and γ -phosphate are expected to be equally involved in $\text{Mg}^{2+}_{(\text{aq})}$ association to $\text{ATP}_{(\text{aq})}$. [36, 37] In enzyme-bound $\text{ATP}_{(\text{aq})}$, the β - and γ -phosphate units are most likely to interact with $\text{Mg}^{2+}_{(\text{aq})}$. [14] The binding constants associated with specific Mg^{2+} - $\text{ATP}_{(\text{aq})}$ ion

pairing motifs alter the Gibbs free energy of hydrolysis,[38] as they determine the concentration of each of the species involved in the reaction.

In addition, the relatively small size of the $\text{Mg}^{2+}_{(\text{aq})}$ ion facilitates coordination to multiple phosphate units within $\text{ATP}_{(\text{aq})}$, leading to phosphate-phosphate interactions *via* the negatively charged O sites.[39] These bonding interactions result in charge-distribution changes at the P-O-P bond[31] and differences in electron binding energies (BEs) of the α -, β -, and γ -phosphates in $\text{ATP}_{(\text{aq})}$ and Mg^{2+} - $\text{ATP}_{(\text{aq})}$. Such intramolecular (and intermolecular) charge redistributions, in addition to solvation effects, are reflected in the phosphorylation and dephosphorylation reaction mechanisms.[31, 32, 35, 40]

With that in mind, this study seeks to probe Mg^{2+} - $\text{ATP}_{(\text{aq})}$ interactions at physiological pH using liquid-jet photoelectron spectroscopy (LJ-PES).[41, 42] We aim to investigate whether LJ-PES – which has been proven to have the unique ability to probe chemical shifts in inorganic and organic solutes in aqueous environments[43-47] – is sensitive enough to reveal spectral changes due to Mg^{2+} - $\text{ATP}_{(\text{aq})}$ ion pairing and/or complexation. Mg^{2+} -phosphate interactions have

been previously explored using aqueous-phase X-ray emission,[48] infrared,[30] Raman,[49] and nuclear magnetic resonance (NMR)[50] spectroscopies. The Mg^{2+} - $\text{ATP}_{(\text{aq})}$ coordination chemistry has been recently investigated in the gas phase using mass spectrometry (in particular, phosphate- Mg^{2+} -adenine interactions)[29] and in acetate solutions[51] using NMR spectroscopy. Previous LJ-PES work focused on the ribose or adenine units in $\text{ATP}_{(\text{aq})}$ [52-54] or on inorganic phosphate[55] aqueous solutions.

Here, we report on the electronic-structure changes upon the addition of Mg^{2+} to $\text{ATP}_{(\text{aq})}$ solutions and the formation of different Mg^{2+} - $\text{ATP}_{(\text{aq})}$ complexes from valence and Mg 2p, Mg 2s, P 2p, and P 2s core-level photoelectron (PE) spectra. The valence spectral region provides information on orbital hybridization due to chemical bonding and ion-pairing interactions, while core-level data reveals site-specific chemical shifts.[43, 56, 57] We also present P 2s spectra from $\text{ATP}_{(\text{aq})}$, $\text{ADP}_{(\text{aq})}$, and $\text{AMP}_{(\text{aq})}$ solutions and investigate relative changes in the BEs of α -, β -, and γ -phosphate with the aid of theoretical calculations. In addition to recording PE spectra upon direct photoionization, we explore the potential of a particular structure-sensitive non-local autoionization probe. Specifically, we report on intermolecular Coulombic decay (ICD)[58-62] of $\text{Mg}^{2+}_{(\text{aq})}$ ions in the presence of $\text{ATP}_{(\text{aq})}$ in their coordination environment (*i.e.*, in the first solvation shell). More precisely, we measure ICD upon photoionization of Mg 1s core-level electrons. Here, the respective core hole is refilled by electrons from the Mg 2s (or Mg 2p) core levels, and the released excess energy is used to ionize the surrounding molecules in the first solvation shell. The emitted secondary electron is then detected as an ICD signal. The ICD spectral region is thus exclusively sensitive to intermolecular interactions, allowing us to directly probe ligand exchange at the Mg^{2+} - $\text{ATP}_{(\text{aq})}$ coordination environment.

Overall, the work presented here provides an element-specific overview of the coordination chemistry of $\text{ATP}_{(\text{aq})}$ in the presence of $\text{Mg}^{2+}_{(\text{aq})}$ and constitutes, to our knowledge, the first report of aqueous-phase PES – including both direct photoionization and non-local autoionization – probing site-specific Mg^{2+} - $\text{ATP}_{(\text{aq})}$ interactions at the phosphate chain and the $\text{Mg}^{2+}_{(\text{aq})}$ coordination sphere.

METHODS

Experiments. 0.5 M $\text{ATP}_{(\text{aq})}$, $\text{ADP}_{(\text{aq})}$, and $\text{AMP}_{(\text{aq})}$ solutions were prepared by dissolving the required amount of adenosine 5'-triphosphate disodium salt hydrate, adenosine 5'-diphosphate acid, and adenosine 5'-monophosphate disodium salt (Carbosynth, 95%) in Millipore water, respectively. $\text{ATP}_{(\text{aq})}$ and $\text{ADP}_{(\text{aq})}$ samples containing Mg^{2+} were prepared by addition of $\text{Mg}(\text{NO}_3)_2$ (ACROS ORGANICS, 99+%) to 0.5 M $\text{ATP}_{(\text{aq})}$ or $\text{ADP}_{(\text{aq})}$ solutions in order to reach 0.25:1, 0.5:1, 0.75:1, 1:1, and 1.5:1 $\text{Mg}^{2+}/\text{ATP}$ concentration ratios. For each sample, the solution pH was adjusted to 8.2 by the addition of the required amount of Tris [tris(hydroxymethyl)aminomethane, Sigma Aldrich, $\geq 99.8\%$], to ensure that the $\text{ATP}_{(\text{aq})}$ phosphate chain was fully deprotonated ($\text{ATP}^{4-}_{(\text{aq})}$, see Figure 1).[19, 22, 63] This alternative approach to the traditional Tris/TrisHCl buffer pH adjustment methodology allows us to reduce the number of chem-

ical species in the solution that can interfere with the observation of the PE signals of interest. The specific concentration of $\text{Tris}_{(\text{aq})}$ in each sample is listed in Table S1 in the Supporting Information (SI).

LJ-PES experiments were performed at the P04 beamline at PETRA III[64] (DESY, Hamburg, Germany) using the EASI setup.[65] Photoelectrons emitted from the sample were detected using a differentially pumped hemispherical electron analyzer at 130° with respect to the light propagation axis (circular polarization). The samples were delivered into the vacuum chamber of the EASI setup in the form of liquid microjets[66] using a glass capillary of 28 μm inner diameter and flow rates in the range of 0.55-0.80 mL/min. The sample temperature was kept at 10°C by means of a cooling system interfaced with the liquid-jet holder. In addition, a small metallic tube was placed into the main polyether ether ketone (PEEK) liquid delivery line to electrically connect and ground the liquid jet to EASI. The liquid jet's (horizontal) flow axis was perpendicular to both the light propagation (floor plane) and the electron detection (at an angle of 130° with respect to the photon beam) axes. PE spectra from $\text{ATP}_{(\text{aq})}$ with dissolved Mg^{2+} were recorded using a photon energy of 250 eV, spanning over the valence, Mg 2p, Mg 2s, P 2p, and P 2s spectral regions. P 2s PE spectra from $\text{AMP}_{(\text{aq})}$, $\text{ADP}_{(\text{aq})}$, and $\text{ATP}_{(\text{aq})}$ were recorded using a photon energy of 330 eV. ICD experiments were performed at 1314 eV. The overall instrumental energy resolution was, approximately, 210 meV at 250 eV, 220 meV at 330 eV, and 570 meV at 1314 eV photon energy.

The BE scale in the data presented here was calibrated based on the liquid water $1b_1$ BE of 11.33 eV,[67] as commonly adopted in LJ-PES experiments.[68] While we have recently reported a more robust methodology,[67] the data acquisition of the results presented here precede those experiments. Furthermore, absolute BEs are not the principal quantity of interest in this work, but rather relative spacing of peaks identifiable to different species in solution.

Computations. α -, β -, and γ -phosphate P 2s BEs of $\text{ATP}^{4-}_{(\text{aq})}$ (as $\text{NaATP}^{3-}_{(\text{aq})}$), $[\text{MgATP}]^{2-}_{(\text{aq})}$, $\text{Mg}_2\text{ATP}_{(\text{aq})}$, and $[\text{MgADP}]^{-}_{(\text{aq})}$, as well as $\text{Mg}^{2+}_{(\text{aq})}$, were calculated using the maximum-overlap method[69] as implemented in the Q-Chem 6.0 software[70] (the sample input for these calculations can be found in the SI). An excellent computational cost/performance ratio was previously demonstrated with this approach.[71] Due to the system size, we pragmatically employed the Hartree-Fock (HF) method with a core-enhanced aug-cc-pCVTZ basis set on P atoms and aug-cc-pVTZ basis set on other atoms. To model Mg 2s and 2p BEs, a core-enhanced aug-cc-pCVTZ basis set was used for Mg atoms and aug-cc-pVTZ for other atoms. The aqueous solution was modeled by the cluster-continuum approach. For our quantum system, we explicitly included 26 water molecules around the triphosphate chain (to cover each terminal O with at least three hydrogen bonds from water molecules) of $\text{ATP}^{4-}_{(\text{aq})}$, $[\text{MgATP}]^{2-}_{(\text{aq})}$, $\text{Mg}_2\text{ATP}_{(\text{aq})}$, and $[\text{MgADP}]^{-}_{(\text{aq})}$ to screen the high charge density while the rest of the solvent was described by the polarizable-continuum model (PCM).[72, 73] We used the non-equilibrium variant of PCM with integral-equation formalism (IEF), Bondi radii, and recommended scaling factor $\alpha = 1.2$.[74] For pure $\text{Mg}^{2+}_{(\text{aq})}$

solutions, the cation was solvated by six explicit water molecules in an octahedral geometry, while the rest of the solvent was modeled by PCM. The calculated P 2s BEs (using HF) were corrected for the correlation as follows. We used pyrophosphate ($\text{HP}_2\text{O}_7^{2-}$) hydrated by five explicit water molecules as a smaller model of the phosphate chain in our $\text{ATP}^{4-}_{(\text{aq})}$, $[\text{MgATP}]^{2-}_{(\text{aq})}$, $\text{Mg}_2\text{ATP}_{(\text{aq})}$, and $[\text{MgADP}]^{-}_{(\text{aq})}$ systems. We computed the P 2s BEs using the HF and MP2 methods to approximately determine the error connected to the missing correlation in the HF method. The correction was estimated to be +0.33 eV. The calculations of BEs were done on single structures optimized on the HF/6-31+G* level of theory with PCM (IEF, Bondi radii, $\alpha = 1.2$) using Gaussian 09, revision D.01[75] (the Cartesian coordinates can be found in the SI).

RESULTS AND DISCUSSION

Element-specific overview of Mg^{2+} - $\text{ATP}_{(\text{aq})}$ interactions. This section presents valence and core-level PE spectra from $\text{ATP}_{(\text{aq})}$ samples with dissolved Mg^{2+} , providing an overview of the electronic structure of $\text{ATP}_{(\text{aq})}$ and the interactions between the metal cation and different units in the $\text{ATP}_{(\text{aq})}$ molecule.

PE spectra from 0.5 M $\text{ATP}_{(\text{aq})}$ solutions with $\text{Mg}^{2+}_{(\text{aq})}$ at different $\text{Mg}^{2+}/\text{ATP}$ concentration ratios recorded at a photon energy of 250 eV are presented in Figure 2. For each sample, the data spans over the valence, Mg 2p,

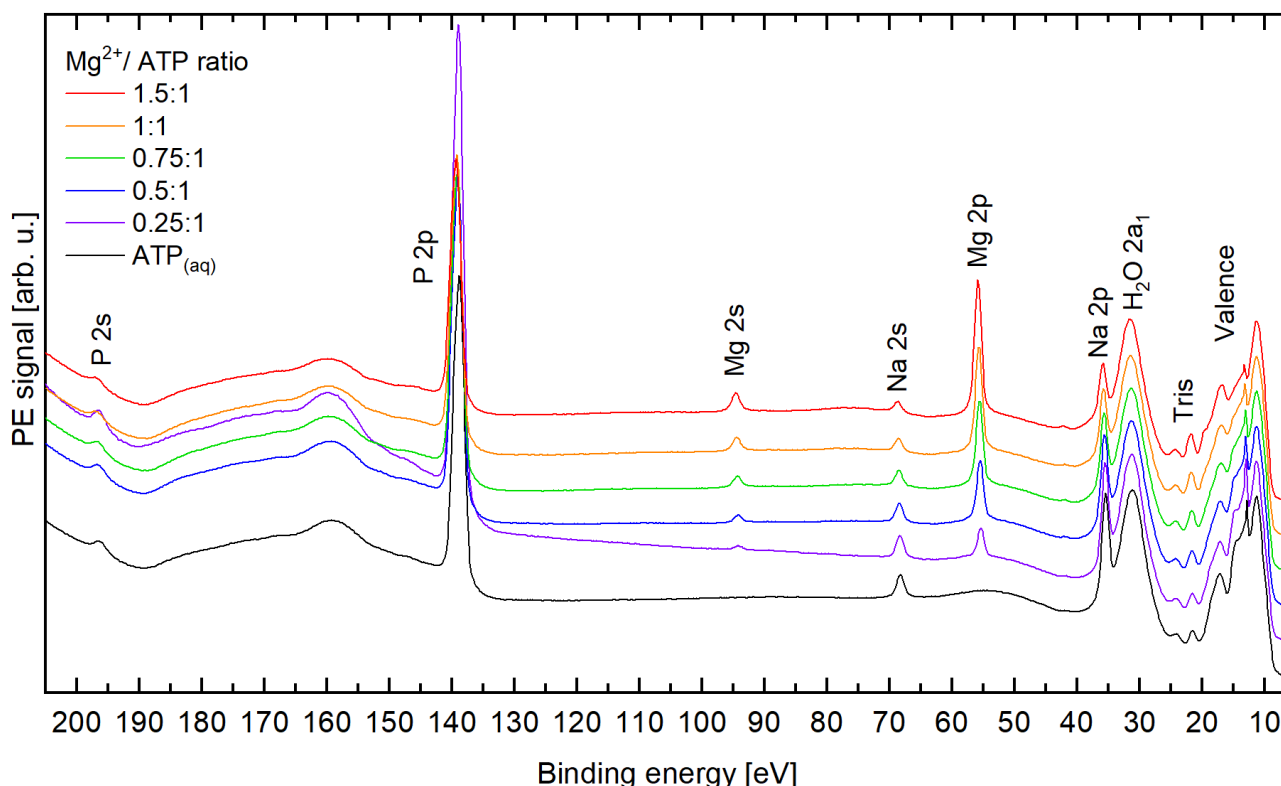


Figure 2. Valence as well as Mg 2p, Mg 2s, P 2p, and P 2s core-level PE spectra from $\text{ATP}_{(\text{aq})}$ samples containing $\text{Mg}^{2+}_{(\text{aq})}$ as a function of the $\text{Mg}^{2+}/\text{ATP}$ concentration ratio. The BE scale was calibrated based on the liquid-water solvent valence $1b_1$ peak position, and spectral intensities are displayed to yield its same height. A vertical offset was applied to each spectrum to facilitate a better comparison between the different data sets. The broad signals close to 160 eV and ~ 55 eV likely originate from energy-loss peaks.[76]

Mg 2s, P 2p, and P 2s spectral regions in a single scan. Similar data recorded from 0.5 M $\text{ATP}_{(\text{aq})}$ without $\text{Mg}^{2+}_{(\text{aq})}$ is shown for comparison. The as-measured spectra are energy-calibrated against the liquid water $1b_1$ peak at 11.33 eV,[67] and intensities are displayed to yield the same liquid water $1b_1$ peak heights. The differences in baseline height are due to slight jet instabilities inherent to the measurements. Spectral features from the $\text{Na}^{+}_{(\text{aq})}$ counter ion in the ATP salt used to prepare the solutions are labeled according to Reference[77]. The intensity of these features is

observed to decrease as the $\text{Mg}^{2+}_{(\text{aq})}$ concentration increases. The reason is not understood but might be due to changing propensity of the solute under study at the surface. Contributions from the $\text{NO}_3^{-}_{(\text{aq})}$ counter ion from the Mg salt used in the experiments are expected in the 9-9.5 eV BE range.[41] Contributions from Tris added to adjust the pH are labeled based on Reference[47] and valence PE data

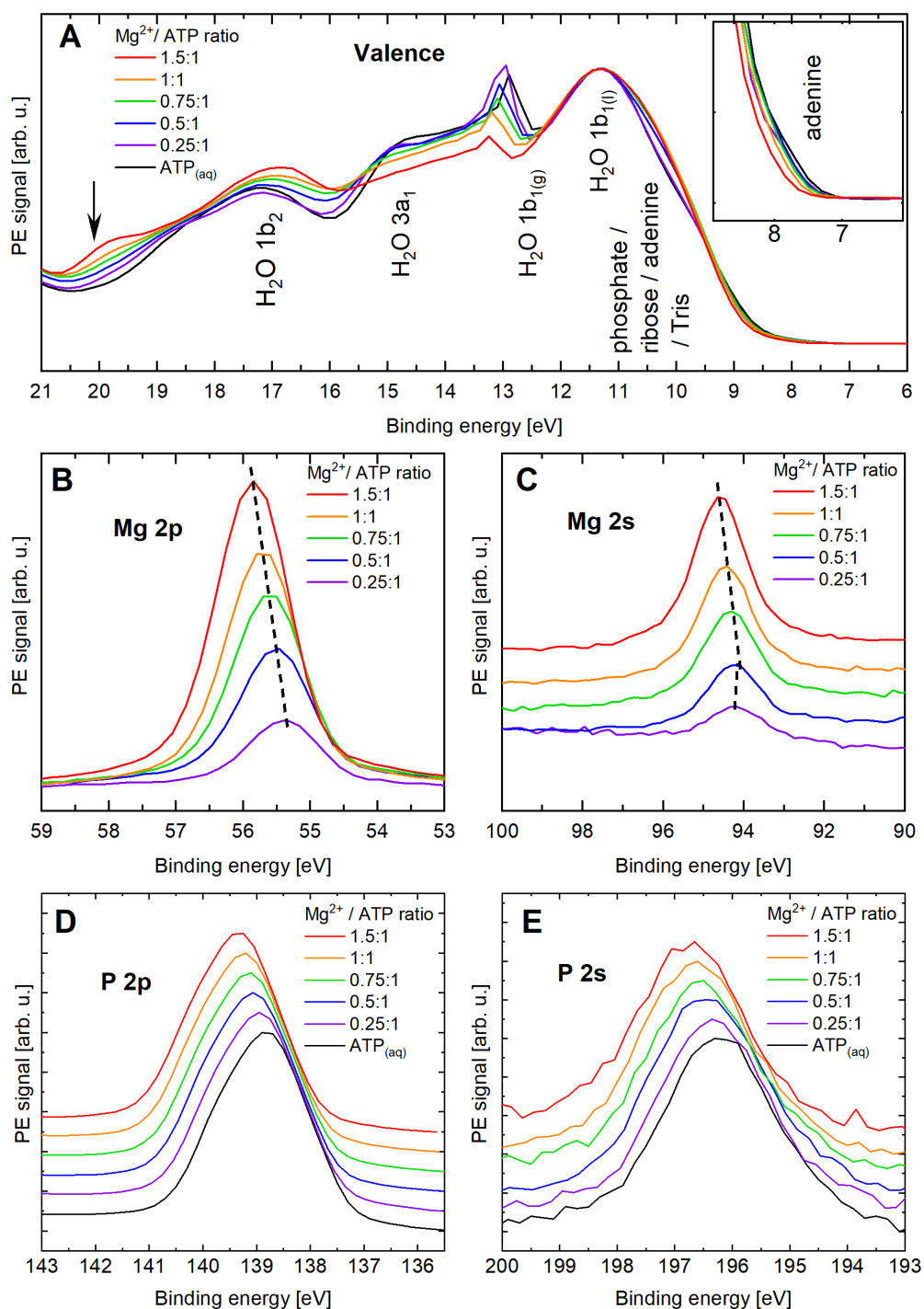


Figure 3. Highlights of the valence [panel (a)], Mg 2p [panel (b)], Mg 2s [panel (c)], P 2p [panel (d)], and P 2s [panel (e)] spectral regions from the data presented in Figure 2. In panel (a), PE signatures of ionization of water's valence electrons are labelled as (liquid- and gas-phase) 1b₁, 3a₁, and 1b₂, according to Reference[76]. The arrow highlights PE signatures due to Mg²⁺-phosphate interactions, as explained in the text. The Mg 2s, P 2p, and P 2s data are shown with a vertical offset for a better comparison, and chemical shifts are highlighted by the dashed lines. The P 2p and P 2s data were normalized in intensity, considering that the ATP_(aq) concentration remains constant across those data sets (as opposed to the Mg²⁺_(aq) concentration in the Mg 2p and Mg 2s spectra, whose variation is reflected in the peak intensities). Linear baselines were subtracted from the P 2s data to remove the secondary electron background (see Figure S5 in the SI for details).

recorded from $\text{Tris}_{(\text{aq})}$ solutions (see Figure S2 in the SI). A highlight of each spectral region is shown in Figure 3 [panels (a)-(e)].

Figure 3(a) focuses on the valence region, which is dominated by PE signatures of ionization of water valence electrons,[76] labeled as (liquid- and gas-phase) $1b_1$, $3a_1$, $1b_2$, and $2a_1$ (the latter only included in Figure 2). Observed energy shifts and intensity variations of the $1b_{1(g)}$ peak can be assigned to a weak charging of the liquid-jet surface upon addition of solute[65]. Based on a valence LJ-PES study of $\text{AMP}_{(\text{aq})}$ published previously[47] and valence PE spectra from $\text{ADP}_{(\text{aq})}$ and $\text{ATP}_{(\text{aq})}$ (see Figure S3 in the SI for details), the phosphate, ribose, and adenine PE signatures are present in the 8-10 eV BE range, with an additional adenine feature also present at 7-8 eV, as highlighted in the figure inset in Figure 3(a).

The adenine feature at 7-8 eV BE in Figure 3(a) is observed to shift as the $\text{Mg}^{2+}/\text{ATP}$ concentration ratio increases. Similar shifts are observed in valence PE spectra recorded from $\text{ADP}_{(\text{aq})}$ solutions as a function of the $\text{Mg}^{2+}/\text{ADP}$ concentration ratio (see Figure S4 in the SI). Such a spectral shift might be a signature of the previously and aforementioned speculated water-mediated Mg^{2+} -adenine interactions in $[\text{MgATP}]^{2-}_{(\text{aq})}$ [17, 18], possibly associated with some closed-structure form, as depicted in Figure 1(b). Furthermore, gas-phase mass spectrometry experiments have shown the presence of phosphate- Mg^{2+} -adenine interactions in both Mg^{2+} -ATP and Mg^{2+} -ADP complexes, although no water is involved in the complexes.[29] One could argue that for the closed-form structure, the metal-ion-bound water molecule donates a hydrogen bond to the N atom of adenine, causing the observed increase in its BE, leading to a cation-stabilized electron in the highest occupied molecular orbital (HOMO) in the adenine moiety.

Signals at higher BEs associated with adenine and ribose orbitals are expected in the 10-20 eV BE range.[78] Furthermore, the emergence of an additional feature is evident close to 20 eV BE at the highest $\text{Mg}^{2+}/\text{ATP}$ concentration ratio [see the arrow in Figure 3(a)]. This spectral change could potentially result from the presence of Mg^{2+} -phosphate interactions in any of the Mg^{2+} - $\text{ATP}_{(\text{aq})}$ moieties presented in Figure 1 and Figure S1, in which O atoms from the phosphate chain are directly exposed to the positive charge from the divalent cation. Previous LJ-PES experiments have been shown to be sensitive to Na^+ -phosphate electrostatic interactions,[55] and we expect the presence of $\text{Mg}^{2+}_{(\text{aq})}$ to have a more pronounced effect. To understand the identity of the orbitals involved in this ionization feature, the inner-valence region was explored using the same methodology used to calculate P 2s BEs as reported in the computations section. Our results indicate that the 20 eV BE feature originates from ionization of electrons from mixed, delocalized molecular orbitals appearing when $\text{Mg}^{2+}_{(\text{aq})}$ ions are closely bound to the phosphate chain, with significant contributions from O, C, and P atoms. We note that O 2s signatures from phosphate compounds are expected in the 24-25.7 eV BE range[79] and are likely hidden underneath the water $2a_1$ peak.

For samples containing $\text{Mg}^{2+}_{(\text{aq})}$, the Mg 2p and Mg 2s PE features occur near 55 eV and 95 eV and are highlighted in Figures 3(b) and 3(c), respectively. With increasing $\text{Mg}^{2+}/\text{ATP}$ concentration ratio, the respective intensities increase, and the peak centers shift to higher BEs; these shifts are indicated by dashed lines. We observe similar trends in the P 2p and P 2s spectral regions, near 140 and 196 eV BEs, as highlighted in Figures 3(d) and 3(e).

A quantitative analysis of the evolution of the observed chemical shifts is presented in Figure 4(a). Note that we can include a data point at zero Mg^{2+} concentration only for the P 2p and P 2s analyses. Although these BEs, from aqueous solutions containing only Mg^{2+} , have been reported previously,[61] connecting those values with the present data is not straightforward. This is due to the inherent experimental error in determining accurate absolute BEs when calibrating to peak positions measured from neat liquid water, and thus neglecting solute-induced effects on the water electronic structure; see again footnote §. Such effects have been recently quantified for a few representative aqueous solutions, based on the simultaneous detection of the low-energy cut-off of the respective PE spectrum.[67] However, this method could not be applied for the work presented here, and was not applied in Reference [61] either, so the two works may have an error in absolute BE of up to 200 meV that prohibits accurate cross-comparison. While uncertainties in the absolute BEs shown in Figure 4(a) are up to 200 meV, and, as the data shown in Figure 3, were all taken at the same time, the relative shifts should be meaningful. For the Mg 2p and Mg 2s data in Figure 4(a), we have thus assumed that for the lowest $\text{Mg}^{2+}/\text{ATP}$ concentration ratio of 0.25, the chemical shift is negligibly small (well justified for a non-surface-active molecule,[80] corresponding to zero energy shift). The small minimum in the Mg 2s data at the 0.50 ratio implies some deviation from the main trend of increasing chemical shift, which is in agreement with our calculations as we further detail below. Despite these experimental constraints, the results of Figure 4(a) show that Mg and P core-level LJ-PES is indeed sensitive to Mg^{2+} -phosphate interactions in $\text{ATP}_{(\text{aq})}$.

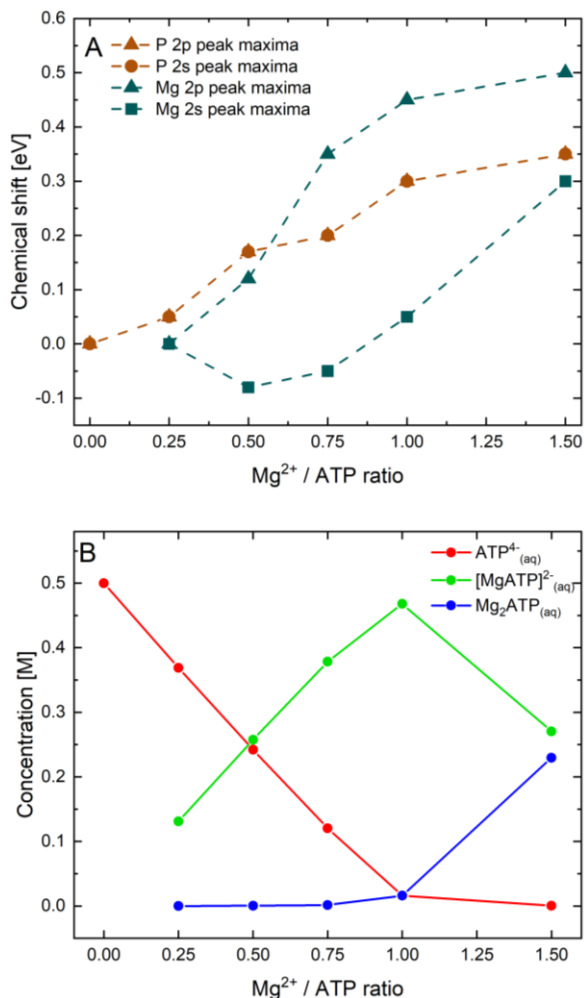


Figure 4. (a) Chemical shifts extracted from the Mg 2p, Mg 2s, P 2p, and P 2s core-level data presented in Figure 3 [panels (b)-(e)] as a function of the Mg²⁺/ATP concentration ratio. (b) Molar concentration of the predominant species – ATP⁴⁻(aq), [MgATP]²⁻(aq), and Mg₂ATP(aq) as a function of the Mg²⁺/ATP concentration ratio at a solution pH of 8.2 calculated within this work using equilibrium constants from Reference[22]. Details on the procedure can be found in the SI.

Figure 4(a) thus suggests that the BEs of all four core levels exhibit a clear positive chemical shift, up to 300-500 meV for the highest Mg²⁺/ATP concentration ratios. There is no indication from the present data of any orbital-character-specific sensitivity in the case of P core levels due to Mg²⁺-ATP(aq) interactions. On the other hand, such an effect appears to be revealed for Mg core levels, where chemical shifts in the Mg 2p BEs tend to be larger than for the Mg 2s counterparts (with the exception of the 0.25 concentration ratio); this may point to the more directional bonding of the outermost 2p orbital.

We next discuss why both P and Mg core-level BEs shift in the same positive direction. Phosphate P core-level BEs are stabilized by the interaction with Mg²⁺(aq), as expected based on simple electrostatic arguments. For Mg²⁺(aq), the

chemical shifts are either non-monotonous (2s) or of increasing BE (2p), starting already at small Mg²⁺(aq) concentrations.

To investigate this behavior, we performed calculations of Mg 2s and 2p BEs. The results are presented in Table 1. Our computations suggest a decrease in BEs when moving from pure Mg²⁺(aq) to [MgATP]²⁻(aq) and an increase in BE when moving to [Mg₂ATP]²⁻(aq). This would be in agreement with the minimum in the Mg 2s data in Figure 4a. But in the absence of reference measurements of Mg 2s and 2p spectra from Mg²⁺(aq) solutions without ATP, there is not enough experimental evidence for the theoretically predicted behavior at low Mg²⁺(aq) concentration. The predicted effect on chemical shifts is approximately the same for Mg 2s and Mg 2p. Therefore, the experimentally observed orbital-character-sensitivity for Mg core levels remains to be explained. Furthermore, note that the calculated difference in Mg core-level BEs for [MgATP]²⁻(aq) and [Mg₂ATP]²⁻(aq) is somewhat higher (approximately 800 meV) compared to the experiment (approximately 300-500 meV). We attribute this discrepancy to the level of computational theory. Importantly, the trends are well reproduced.

	Mg 2s	Mg 2p
Mg ²⁺ (aq)	96.01	55.24
[MgATP] ²⁻ (aq)	95.21	54.42
[Mg ₂ ATP] ²⁻ (aq)	96.08	55.30

We have also estimated the solution composition of the Mg²⁺/ATP(aq) samples studied here using the binding constants of different Mg²⁺-ATP(aq) complexes reported in Reference[22] (see the SI for details, including Table S2). While these values refer to lower ionic-strength conditions compared to the samples studied in this work, our primary focus is to produce a first-order approximation speciation plot to guide our qualitative description of the data. We have estimated that ATP⁴⁻(aq) and [MgATP]²⁻(aq) (see Figure 1) are the dominant species at Mg²⁺/ATP concentration ratios between 0.25:1 and 0.75:1, with an increasing proportion of [MgATP]²⁻(aq) as the concentration of Mg²⁺ increases. At a 1:1 Mg²⁺/ATP ratio, there is no longer free ATP(aq) (ATP⁴⁻(aq)) in solution, and [MgATP]²⁻(aq) is the prevailing species. At a 1.5:1 Mg²⁺/ATP ratio, the [MgATP]²⁻(aq) concentration decreases as the formation of [Mg₂ATP]²⁻(aq) becomes relevant (see Figure S1 in the SI). The amount of free Mg²⁺(aq) was estimated to be negligible at all the Mg²⁺/ATP concentration ratios studied here. The results are summarized in Figure 4(b). We consider this to be a minimal set of species expected in significant amounts in the prepared solutions influenced by the speciation analysis of Reference[22]. For instance, to simplify, we have omitted [Mg(ATP)₂]⁶⁻(aq), although this species may contribute to the signal at the lower Mg²⁺ concentrations[23].

As listed in Table S1 in the SI, it was necessary to increase the $\text{Tris}_{(\text{aq})}$ concentration in our samples with the $\text{Mg}^{2+}/\text{ATP}$ ratio to maintain a constant solution pH of 8.2. One potential concern might be that $\text{Mg}^{2+}_{(\text{aq})}$ binding to $\text{Tris}_{(\text{aq})}$ would impact speciation with $\text{ATP}_{(\text{aq})}$. However, $\text{Mg}^{2+}_{(\text{aq})}$ complexation to $\text{Tris}_{(\text{aq})}$ is known to be weak compared to other divalent cations, such as $\text{Cu}^{2+}_{(\text{aq})}$, [81] and the binding constant of $\text{Tris}_{(\text{aq})}$ with $\text{Cu}^{2+}_{(\text{aq})}$ is 2-4 orders of magnitude lower than those for $[\text{MgATP}]^{2-}_{(\text{aq})}$ and $\text{Mg}_2\text{ATP}_{(\text{aq})}$ (as listed in the SI). Hence, we expect the valence (and Mg core-level) spectral changes observed as a function of the $\text{Mg}^{2+}/\text{ATP}$ concentration ratio to be predominantly accounted for the formation of $[\text{MgATP}]^{2-}_{(\text{aq})}$ and $[\text{Mg}_2\text{ATP}]_{(\text{aq})}$. Consequently, the valence spectral changes and core-level chemical shifts observed in Figures 2 and 3 can be attributed to the presence of $[\text{MgATP}]^{2-}_{(\text{aq})}$ and $[\text{Mg}_2\text{ATP}]_{(\text{aq})}$ in increasing proportion at each $\text{Mg}^{2+}/\text{ATP}$ ratio.

Notably, at the sample concentrations employed here, any Mg^{2+} -phosphate interactions observed in our data can also correspond to phosphate- Mg^{2+} -phosphate intramolecular bridges between $\text{ATP}_{(\text{aq})}$ molecules, which are expected to occur at concentrations above 10^{-3} M. [82, 83]. Nevertheless, the presence of deprotonated sites on the phosphate chain (as in the samples studied here, where $\text{ATP}_{(\text{aq})}$ is expected to be fully deprotonated) reduces the formation of such bridges due to repulsion interactions between the negatively charged O atoms. [83] Furthermore, our ICD measurements to be discussed below show no evidence for the bridged structure.

α -, β -, and γ -phosphate-specific interactions in $\text{ATP}_{(\text{aq})}$ and Mg^{2+} - $\text{ATP}_{(\text{aq})}$. Here, we focus on the question of whether it is possible to discriminate α -, β -, and γ -phosphate units in the $\text{ATP}_{(\text{aq})}$ phosphate chain on the basis of PE spectra. As a starting point, we performed computations to calculate the P 2s BEs of each phosphate unit in fully deprotonated $\text{ATP}_{(\text{aq})}$ ($\text{ATP}^{4-}_{(\text{aq})}$), as found at the solution pH of the samples studied here. We obtained nearly identical α - and β -phosphate P 2s BEs (196.93 eV and 196.97 eV, respectively), and an ~ 850 -900 meV lower γ -phosphate P 2s BE (196.08 eV). In agreement with a previous report on P 2p PES from solid-phase calcium tripolyphosphate, [84] our results show that the bridging phosphate groups (α and β units) have higher BEs than the terminal phosphate (γ -phosphate). In $\text{ATP}^{4-}_{(\text{aq})}$, P core-level electrons in the γ -phosphate are uniquely subjected to repulsive interactions from two negatively charged O sites, while α and β units contain a single deprotonated site [see Figure 1(a)]. Such differences in the local chemical environment lead to lower γ -phosphate P 2s BE values compared to the α and β units. (We note that the present and following discussions do not extend to P 2p BEs since the expected doublet peak-structure would prevent a similarly accurate distinction of the small energetic differences associated with the specific phosphate groups.)

With this information in mind, we attempted to deconvolve P 2s PE spectra recorded from $\text{ATP}_{(\text{aq})}$ samples into individual α -, β -, and γ -phosphate contributions with the aid

of spectra from $\text{AMP}_{(\text{aq})}$ and $\text{ADP}_{(\text{aq})}$. When discussing the respective electron BEs, it is useful to refer to each phosphate group as adenosine-phosphate bridging unit, terminal unit, and phosphate-phosphate bridging unit, rather than α -, γ -, and β -, respectively; this characterization most directly reflects the origin of the different BEs, as described below.

Figure 5 shows P 2s PE spectra from 0.5 M $\text{AMP}_{(\text{aq})}$ (magenta curve), $\text{ADP}_{(\text{aq})}$ (cyan curve), and $\text{ATP}_{(\text{aq})}$ (black curve) solutions at pH 8.2 recorded using a photon energy of 330 eV. A linear baseline was subtracted from each spectrum, and the BE scale was calibrated with respect to the liquid water $1b_1$ feature [67] in valence data recorded under similar conditions. P 2s peak areas extracted from Voigt profile fits were used to re-scale the signal intensities of the $\text{ADP}_{(\text{aq})}$ and $\text{ATP}_{(\text{aq})}$ spectra to twice ($\text{ADP}_{(\text{aq})}$) and three times ($\text{ATP}_{(\text{aq})}$) with respect to the $\text{AMP}_{(\text{aq})}$ spectrum, based on the number of phosphate units in each case. Further details regarding the data treatment are presented in Figure S6 in the SI.

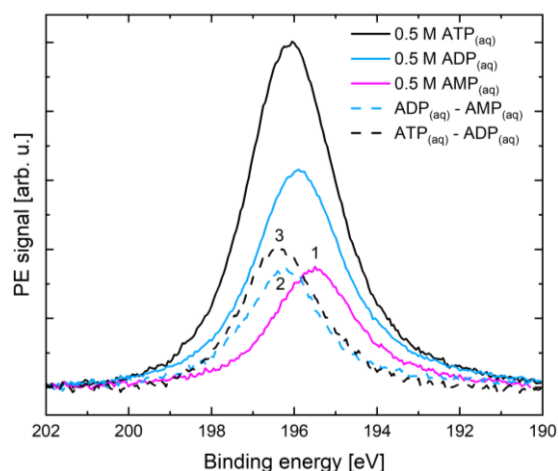


Figure 5. P 2s PE spectra recorded from $\text{AMP}_{(\text{aq})}$, $\text{ADP}_{(\text{aq})}$, and $\text{ATP}_{(\text{aq})}$ solutions without dissolved Mg^{2+} . The $\text{AMP}_{(\text{aq})}$ data is representative of a terminal phosphate (peak 1), while bridging phosphate units in $\text{ATP}_{(\text{aq})}$ (peaks 2 and 3) were identified by subtracting the $\text{AMP}_{(\text{aq})}$ data from the $\text{ADP}_{(\text{aq})}$ spectrum (cyan dashed line) and the $\text{ADP}_{(\text{aq})}$ data from the $\text{ATP}_{(\text{aq})}$ spectrum (black dashed line).

A BE of 195.3 eV (peak 1 in Figure 5) was determined for $\text{AMP}_{(\text{aq})}$, corresponding to its single (terminal) phosphate group. Given that the $\text{ADP}_{(\text{aq})}$ phosphate chain contains two phosphate units, a second phosphate BE (peak 2) was determined by subtracting the $\text{AMP}_{(\text{aq})}$ spectrum from the $\text{ADP}_{(\text{aq})}$ data. The difference spectrum is shown using a cyan dashed line. A similar approach was implemented to determine the BE of a third phosphate unit (peak 3) by producing the $\text{ATP}_{(\text{aq})}$ - $\text{ADP}_{(\text{aq})}$ difference spectrum, shown using a black dashed line in Figure 5. Voigt profile fits to the difference spectra revealed BEs of 196.2 eV and 196.3 eV for peak 2 and 3, respectively (see Figure S6 in the SI).

As mentioned in the experimental section, we consider the methodology applied here to provide only relative BE values rather than absolute values. Hence, we determined BE energy differences of 900 meV between peaks 1 and 2, and 100 meV between peaks 2 and 3, in agreement with our computations. Based on these results, we assign peak 1 as a PE signature of the terminal phosphate (γ) in $\text{ATP}_{(\text{aq})}$, and peaks 2 and 3 as PE signatures of bridging phosphate units. In doing so, we are assuming that the terminal phosphate P 2s BE value is the same in $\text{AMP}_{(\text{aq})}$, $\text{ADP}_{(\text{aq})}$, and $\text{ATP}_{(\text{aq})}$. The other two phosphate groups, the adenosine-phosphate bridging (α) moiety and the phosphate-phosphate bridging (β) unit, correspond each to different chemical environments, associated with different P 2s BEs.

To assign the BEs extracted from peaks 2 and 3 to such moieties, and to evaluate our assumption more generally, we calculated the P 2s BEs of the individual phosphate units in $\text{ADP}_{(\text{aq})}$ ($[\text{MgADP}]_{(\text{aq})}$). Our results confirm that the terminal phosphate in $\text{ADP}_{(\text{aq})}$ has a lower BE (196.04 eV) compared to the bridging phosphate attached to the nucleoside (196.80 eV). With that in mind, we can assign peaks 2 and 3 as β - and α -phosphate in $\text{ATP}_{(\text{aq})}$, respectively. Our calculations also show that our assumption of the BE values of the terminal phosphate units in $\text{ADP}_{(\text{aq})}$ and $\text{ATP}_{(\text{aq})}$ being of the same magnitude is valid.

In addition, we investigated the effect of Mg^{2+} -phosphate interactions on the P core-level BEs of each individual phosphate group in $\text{ATP}_{(\text{aq})}$ by calculating the P 2s BEs of α -, β -, and γ -phosphate of $[\text{MgATP}]^{2-}_{(\text{aq})}$ and $\text{Mg}_2\text{ATP}_{(\text{aq})}$. For $[\text{MgATP}]^{2-}_{(\text{aq})}$, we considered two different binding motifs – the cation simultaneously bound to the three phosphate units and the cation bound only to the β - and γ -phosphate groups. The results are summarized in Table 2. Overall, we observe an increase in the P 2s BEs due to Mg^{2+} -phosphate interactions, in agreement with the experimental results from the previous section. For all phosphate units in $[\text{MgATP}]^{2-}_{(\text{aq})}$, changes in the number of phosphate groups interacting with $\text{Mg}^{2+}_{(\text{aq})}$ lead to BE differences of ~ 100 meV between the two binding motifs cases. On the other hand, binding to a second $\text{Mg}^{2+}_{(\text{aq})}$ ion, as in $\text{Mg}_2\text{ATP}_{(\text{aq})}$, results in the largest increment in the P 2s BEs, as expected due to the additional positive charge from the metal cation. In addition, the presence of Mg^{2+} -phosphate interactions in $[\text{MgATP}]^{2-}_{(\text{aq})}$ and in $\text{Mg}_2\text{ATP}_{(\text{aq})}$ causes the α - and β -phosphate P 2s BEs to adopt different values, as opposed to in $\text{ATP}_{(\text{aq})}$ in the absence of the divalent cation.

	α	β	γ
$[\text{ATP}]^{4-}_{(\text{aq})}$	196.93	196.97	196.08
$[\text{MgATP}]^{2-}_{(\text{aq})}$ (Mg^{2+} -bonding to α -, β -, and γ -phosphate)	197.33	197.15	196.31

$[\text{MgATP}]^{2-}_{(\text{aq})}$ (Mg^{2+} -bonding to β - and γ -phosphate)	197.28	197.01	196.39
$[\text{Mg}_2\text{ATP}]_{(\text{aq})}$	198.27	197.83	196.82

Intermolecular-specific probe of the $\text{Mg}^{2+}_{(\text{aq})}$ coordination environment in the presence of $\text{ATP}_{(\text{aq})}$. The analysis of the $\text{Mg}^{2+}_{(\text{aq})}$ concentration-dependent valence and core-level spectral changes presented in the previous sections provides site-specific information on the Mg^{2+} - $\text{ATP}_{(\text{aq})}$ bonding interactions. The ICD spectra presented in this section are particularly sensitive to interactions between $\text{Mg}^{2+}_{(\text{aq})}$ and its coordination environment, revealing additional insight into the number and identity of its chelating units.

We show that the ICD signal intensity associated with the hydration shell of a charged atomic ion is proportional to the number of hydrating water molecules and, as a result, the ion-water ICD signal decreases upon replacement of a water molecule by a solute component. In this way, we are sensitive to the exchange of water molecules by $\text{ATP}_{(\text{aq})}$ due to the formation of Mg^{2+} - $\text{ATP}_{(\text{aq})}$; this is illustrated in Figure 6a, where one water molecule is replaced by one phosphate group in the first solvation shell of $\text{Mg}^{2+}_{(\text{aq})}$. The associated ICD spectrum further reveals the character of the most involved water orbital,[61] as we discuss later.

The ICD process explored here, and illustrated in Figure 6(b), takes place after the initial photoionization of Mg 1s core-level electrons producing primary photoelectrons e^-_{ph} . The Mg 1s core hole left behind is refilled by electrons from the Mg 2s (or Mg 2p) core levels, and the released excess energy is used to ionize the surrounding molecules – *i.e.*, the water molecules and the chelating phosphate units in the first coordination shell – producing ICD electrons e^-_{ICD} .

Figure 7(a) shows ICD spectra recorded from 0.5 M $\text{Mg}(\text{NO}_3)_2_{(\text{aq})}$ solutions without $\text{ATP}_{(\text{aq})}$ (black line) and with 1:1 and 1.5:1 $\text{Mg}^{2+}/\text{ATP}$ concentration ratios (orange and red lines, respectively). For the 0.5 M $\text{Mg}(\text{NO}_3)_2_{(\text{aq})}$ solutions (no ATP added), the cation exists in its octahedral configuration ($[\text{Mg}(\text{H}_2\text{O})_6]^{2+}_{(\text{aq})}$) (compare Figure 6(a)), regardless of the presence of the counter ion ($\text{NO}_3^-_{(\text{aq})}$).[21, 22] The data were recorded at a constant photon energy of 1314 eV, which was selected so as to exceed the Mg 1s BE (based on Reference[61]). The secondary-electron background was removed by fitting and subsequently subtracting cubic baselines from the different spectral regions. The Mg 2s peak areas extracted from Voigt fits to each data set were used to normalize the signal intensity in all the spectra by scaling the PE signal ordinate based on the $\text{Mg}^{2+}_{(\text{aq})}$ concentration, assuming similar cross sections. In that way, we normalized the data in Figure 7(a) so as to

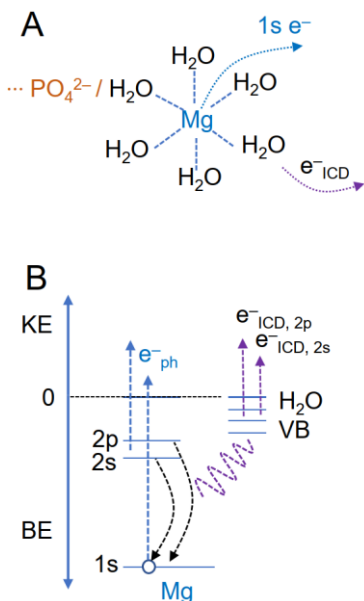


Figure 6. (a) Ejection of the initial 1s photoelectron, $1s e^-$, from $Mg^{2+}_{(aq)}$ and an ICD electron, e^-_{ICD} , associated with the subsequent valence ionization of a hydration-shell water molecule. The sketch also illustrates the direct interaction of $Mg^{2+}_{(aq)}$ with a phosphate unit of $ATP_{(aq)}$ which reduces the number of water molecules in the first solvation shell. (b) Energy level diagram depicting the ICD process. The open circle denotes the 1s core hole upon ionization of Mg^{2+} ; e^-_{ph} are the ejected 1s, 2s, 2p photoelectrons. BE and KE denote electron binding and electron kinetic energies of the measured electrons, respectively. The non-local ICD processes, where the relaxation of the metal core hole involves the first solvation shell, lead to the ionization of all water valence (VB) orbitals (and potentially also of phosphate). This produces the ICD electrons $e^-_{ICD, 2s}$ and $e^-_{ICD, 2p}$.

display the same peak area for the samples where the $Mg^{2+}_{(aq)}$ concentration is 0.5 M (black and orange curves) and an area 1.5 times larger for the sample containing 0.75 M $Mg^{2+}_{(aq)}$ (red curve). In the $Mg^{2+}/ATP_{(aq)}$ data, the energy scale was calibrated with respect to the Na 2p PE peak, which we observe to remain fixed in BE (at 68.3 eV) across all samples in Figure 2. In the $Mg^{2+}_{(aq)}$ -only data, the energy calibration was performed based on the Mg 2s BE value (94.3 eV) reported in Reference[61]. Further details regarding the data treatment can be found in Figure S7 of the SI.

Our first observation is that the Mg 2p and Mg 2s ICD signals occur at slightly but distinctly different KEs in the $Mg^{2+}/ATP_{(aq)}$ spectra with respect to the $Mg^{2+}_{(aq)}$ -only ($[Mg(H_2O)_6]^{2+}_{(aq)}$) data. This directly reflects the formation of $[MgATP]^{2-}_{(aq)}$ (in the 1:1 Mg^{2+}/ATP ratio case) and $Mg_2ATP_{(aq)}$ (in the 1.5:1 Mg^{2+}/ATP ratio case) as discussed in connection with Figure 4(b). The observed spectral changes imply that interactions with $ATP_{(aq)}$ affect the transfer of excess energy from $Mg^{2+}_{(aq)}$ to its coordinating environment during the ICD process, likely due to charge redistribution between the metal ion and the phosphate

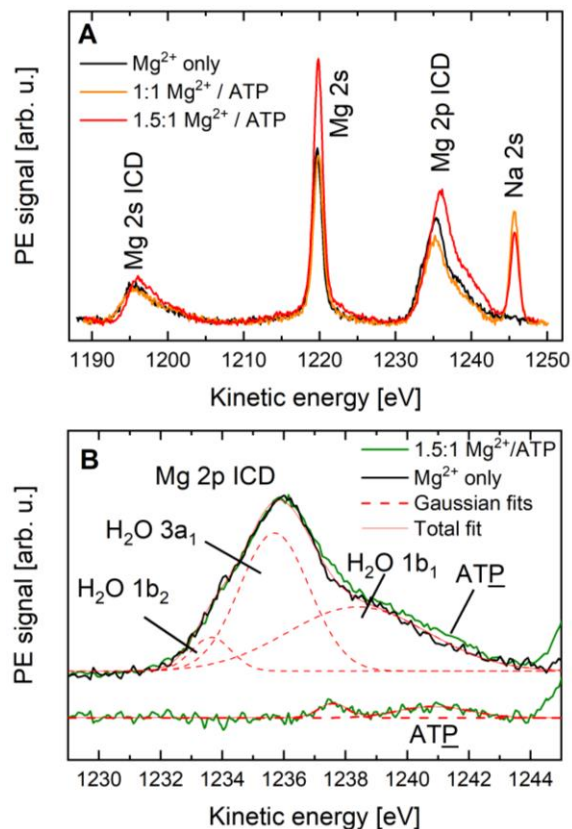


Figure 7. (a) ICD spectra from $Mg^{2+}_{(aq)}$ without $ATP_{(aq)}$ and in the presence of $ATP_{(aq)}$ at 1:1 and 1.5:1 Mg^{2+}/ATP concentration ratios. The signal intensity is shown normalized according to the $Mg^{2+}_{(aq)}$ concentration. The spectral range of the 2s and 2p ICD channels covers the direct Mg 2s ionization. (b) Close-up of the Mg 2p ICD spectral region from the 1.5:1 Mg^{2+}/ATP concentration ratio data presented in panel (a). Spectra are displayed such that the main peaks are at the same KE, and their heights are the same. Gaussian curves (red dashed lines) in the Mg^{2+} only data highlight the individual ionization features from the water orbitals 1b₂, 3a₁, 1b₁ involved in the ICD process. The Mg^{2+}/ATP minus the Mg^{2+} -only difference spectrum shown at the bottom (dark green) reveals the ICD signal associated with the Mg^{2+} -phosphate interaction (labelled ATP).

units in the nucleotide. We note that the $Mg^{2+}_{(aq)}$ -only sample did not contain Tris_(aq), in contrast to the Mg^{2+}/ATP solutions, but Mg^{2+} -Tris_(aq) complexation should be relatively weak, as discussed previously.

Our second observation is that the intensity of the Mg 2p ICD feature decreases in the 1:1 Mg^{2+}/ATP data compared to the $Mg^{2+}_{(aq)}$ -only data, both of which are associated with equal $Mg^{2+}_{(aq)}$ concentrations. This reveals the aforementioned formation of $[MgATP]^{2-}_{(aq)}$ and the associated reduction in the number of the $Mg^{2+}_{(aq)}$ -water ICD channels available. Accordingly, we observe an $\sim 15\%$ reduction in signal intensity. This corresponds to one water molecule out of six being replaced in $[Mg(H_2O)_6]^{2+}_{(aq)}$ upon complexation to

ATP_(aq) (assuming negligible Mg²⁺-Tris_(aq) complexation); compare Figure 6(a). We note that this interpretation implicitly assumes that ICD signals involving phosphate are significantly weaker compared to those involving water.

As expected, based on the Mg²⁺_(aq) concentration in each sample, the intensity of the Mg 2p ICD signal in the 1.5:1 Mg²⁺/ATP data is ~1.5 times higher with respect to the 1:1 Mg²⁺/ATP case. However, if we compare the 1.5:1 Mg²⁺/ATP spectra with the Mg²⁺_(aq)-only data, we observe that the ICD signal intensity in the 1.5:1 Mg²⁺/ATP case is only 1.3 times higher than in the Mg²⁺_(aq)-only case. This shows that the presence of ATP_(aq) causes the signal to change non-linearly with respect to the concentration of the metal cation. In other words, and following our argument from the previous paragraph, we observe an ~15% reduction in signal due to the formation of [MgATP]²⁻_(aq) and Mg₂ATP_(aq).

Another spectral change becomes apparent when overlapping the main peaks (at a common KE and normalized area) of the Mg 2p ICD spectra from both samples, as shown in Figure 7(b) and detailed in the respective figure caption. We recall that the ICD signals are the convolution of ionization peaks associated with all the orbitals involved in the charge-transfer process occurring within the coordination shell. The observed broader Mg 2p ICD feature in the Mg²⁺/ATP spectrum with respect to the Mg²⁺_(aq)-only spectrum thus suggests that the ICD process in the latter involves additional orbitals, other than the water orbitals.[61] In order to test this interpretation, we subtracted the Mg²⁺_(aq)-only data from the 1.5:1 Mg²⁺/ATP data. The difference spectrum is shown in dark green at the bottom of Figure 7(b), highlighting an ICD component associated with ATP (labelled ATP) occurring near 1241 eV KE. Note the occurrence of another feature near 1238 eV, the assignment of which is not clear at the moment. Gaussian fits of the individual water orbitals (1b₂, 3a₁, and 1b₁) to the Mg²⁺_(aq)-only spectrum are shown in dashed lines and are in semi-quantitative agreement with Reference [61]. The ATP contribution from ATP_(aq) interacting with Mg²⁺_(aq), *i.e.*, due to the formation of Mg₂ATP_(aq), is indeed consistent with the lowest phosphate BE being approximately 2 eV lower than that of water 1b₁.[47] As reported previously, Mg²⁺_(aq)-water ICD signals show a high specificity for water electrons from the 3a₁ orbitals.[61] This is also the case for the data presented here, highlighting the sensitivity of the technique to orbital spatial orientation.

Overall, the sensitivity of the ICD signal intensity to the charge of the solvated ion involved in the solute-water energy-transfer process allows us to uniquely probe charge distribution changes upon replacing water molecules in the coordination sphere of [Mg(H₂O)₆]²⁺_(aq) by phosphate from ATP_(aq) to form different Mg²⁺-ATP_(aq) complexes. We note that the ICD spectra do not uncover the water-mediated adenine-Mg²⁺ interaction suggested in the literature since the respective water molecule is one of the constituents in the first hydration shell, with differences in electronic structure with respect to the other water molecules being too small to be detected here.

CONCLUSIONS

We have probed interactions between adenine and phosphate units in ATP_(aq) with Mg²⁺_(aq), as well as the electronic structure of the phosphate chain in ATP_(aq), using LJ-PES plus theoretical calculations and correlating our observations to the formation of [MgATP]²⁻_(aq) and Mg₂ATP_(aq).

Valence PE spectra from solutions with different Mg²⁺/ATP concentration ratios reveal the adenine PE feature in ATP_(aq) to shift in BE as the Mg²⁺_(aq) concentration increases, providing direct evidence of Mg²⁺-adenine and Mg²⁺-phosphate interactions in [MgATP]²⁻_(aq) and Mg₂ATP_(aq).

The Mg 2p, Mg 2s, P 2p, and P 2s PE data demonstrate the element-sensitivity of core-level PES to further support the presence of Mg²⁺-ATP_(aq) interactions in aqueous solution. We report chemical shifts to higher BEs as the Mg²⁺_(aq) concentration increases, with stronger effects for the Mg core levels compared to the P core levels, reflecting the indirect character of Mg-P interactions, which occur *via* O atoms.

We performed a combined analysis of P 2s PE spectra from ATP_(aq), ADP_(aq), and AMP_(aq), and computed BEs to isolate spectral fingerprints of α -, β -, and γ -phosphate in ATP_(aq). Our results reveal that the BEs of the bridging groups in the phosphate chain are higher than that of the terminal phosphate. We also calculated the P 2s phosphate-specific BEs of [MgATP]²⁻_(aq) and Mg₂ATP_(aq), to characterize the effect of different Mg²⁺_(aq)-binding motifs.

Finally, we presented ICD spectra from ATP_(aq) solutions containing Mg²⁺_(aq) at two different concentration ratios, allowing us to probe the interactions between the metal cation and its coordination environment with exceptional sensitivity. From a comparison with Mg²⁺-water ICD features in the absence of ATP_(aq), we detect changes in signal intensity and spectral shape due to the replacement of first-hydration-shell water molecules by phosphate from ATP_(aq).

In summary, the work presented here provides a thorough element-specific overview of Mg²⁺-ATP interactions in aqueous solution on the molecular level. Specifically, the information on the electronic structure, charge distribution, and coordination environment in Mg²⁺-ATP_(aq) complexes offers insight into the molecular aspects underlying phosphorylation and dephosphorylation reactions at physiological pH. In addition, our findings provide insight into the formation of the widely discussed water-mediated Mg²⁺-adenine interactions and while our data is consistent with a closed (ring) Mg²⁺-ATP_(aq) moiety, we cannot rule out the Mg²⁺ ion separately interacting either with adenine or phosphate in the open-form structure.

While we provide a qualitative spectral assignment of Mg²⁺-ATP_(aq) interactions, such information cannot be used, at present, to extend the speciation results reported by Storer *et al.*[22] – which are based on information from pH titration experiments – or to derive thermodynamic information. This is complicated by the very small P 2s BE differences between the α , β , and γ units. Nevertheless, the combined information extracted from the spectral assignments, chemical shifts, and ICD phenomena provides a foundation for potential temperature-dependent PES experiments that

recover the Mg^{2+} -phosphate-dependent Mg^{2+} - $\text{ATP}_{(\text{aq})}$ association equilibria energies and entropy data.

Overall, we have explored the current capabilities of state-of-the-art LJ-PES, including direct PE emission and non-local relaxation processes upon core-level ionization, in characterizing the electronic-structure interactions between ATP and Mg^{2+} in aqueous solution. Future studies will extend the structure-sensitivity of ICD to include the respective P- and N-induced relaxation processes, particularly aiming at providing evidence for the closed-ring structure. Moreover, and in a wider context, we believe that the present results are of relevance to the elucidation of the mechanisms and reaction intermediaries in phosphorylation and dephosphorylation of $\text{ATP}_{(\text{aq})}$ – including the study of the role of $\text{Mg}^{2+}_{(\text{aq})}$ (or $\text{Ca}^{2+}_{(\text{aq})}$) divalent cations as well as the importance of solvation and the role played by specific water molecules.

ASSOCIATED CONTENT

Supporting Information. Additional details regarding sample preparation and predicted speciation, computational methods, treatment and analysis of the PE spectra, and the molecular structures and supporting PE data discussed in the text (PDF). This material is available free of charge via the Internet at <http://pubs.acs.org>. The raw data relevant to this work has been deposited at [10.5281/zenodo.7998786](https://doi.org/10.5281/zenodo.7998786).

AUTHOR INFORMATION

Corresponding Author

*stephen.bradforth@usc.edu, winter@fhi-berlin.mpg.de

Present Addresses

†Sandia National Laboratories California, Livermore, CA 94550, USA

Author Contributions

‡These authors contributed equally.

Notes

§ In the present study, no low-energy cut-off measurements from an electrically biased liquid jet have been performed. This is the reason why we cannot apply the more robust method for a determination of absolute electron binding energies, as recently reported in Reference[67].

ACKNOWLEDGMENT

The authors would like to thank Robert Seidel, Christi Schroeder, Anne B. Stephansen, Claudia Kolbeck, Marvin Pohl, Iain Wilkinson, and Gerard Meijer for their support along different stages of the project and during initial experiments at BESSY II. C.L and D.M. were supported by the Director, Office of Basic Energy Science, Chemical Sciences Division of the U.S. Department of Energy under Contract No. DE-AC02-05CH11231 and by the Alexander von Humboldt Foundation. L.T. and P.S. acknowledge the support of the Czech Science Foundation, project number 21-26601X (EXPRO project). S.B. acknowledges NSF CHE-0617060 for early phases of this work and NSF CHE-1665532 for travel support in finalizing the work. B.W. acknowledges funding from the European Research Council

(ERC) under the European Union's Horizon 2020 research and investigation programme (grant agreement No. 883759). F.T. and B.W. acknowledge support from the MaxWater initiative of the Max-Planck-Gesellschaft. We acknowledge DESY (Hamburg, Germany), a member of the Helmholtz Association HGF, for the provision of experimental facilities. This research was carried out initially at BESSY II (project number 2009_2_90613 at beamline U41-PGM) and subsequently at PETRA III, and we thank Moritz Hoesch as well as the whole beamline staff, the PETRA III chemistry-laboratory and crane operators for assistance in using the P04 soft X-ray beamline.

ABBREVIATIONS

ADP, adenosine diphosphate; AMP, adenosine monophosphate; ATP, adenosine triphosphate; BE, binding energy; HOMO, highest occupied molecular orbital; HF, Hartree-Fock; ICD, intermolecular Coulombic decay; KE, kinetic energy; LJ-PES, liquid-jet photoelectron spectroscopy; NMR, nuclear magnetic resonance; PCM, polarizable continuum model; PE, photoelectron; PEEK, polyether ether ketone; PES, photoelectron spectroscopy; Tris, (tris(hydroxymethyl)aminomethane).

REFERENCES

1. Boyer, P.D., Energy, life, and ATP. Nobel Lecture, December 8, 1997, in Nobel Lectures Chemistry 1996 - 2000, I. Grenthe, Editor. 2003, World Scientific.
2. Kamerlin, S.C.L., et al., Why nature really chose phosphate. Quarterly Reviews of Biophysics, 2013. **46**(1): p. 1-132.
3. Müller, W.E.G., H.C. Schröder, and X. Wang, Inorganic Polyphosphates As Storage for and Generator of Metabolic Energy in the Extracellular Matrix. Chemical reviews, 2019. **119**(24): p. 12337-12374.
4. Bonora, M., et al., ATP synthesis and storage. Purinergic Signalling, 2012. **8**(3): p. 343-357.
5. Zimmerman, J.J., A. von Saint André-von Arnim, and J. McLaughlin, Chapter 74 - Cellular Respiration, in Pediatric Critical Care (Fourth Edition), B.P. Fuhrman and J.J. Zimmerman, Editors. 2011, Mosby: Saint Louis. p. 1058-1072.
6. Sigel, H. and R. Griesser, Nucleoside 5'-triphosphates: self-association, acid-base, and metal ion-binding properties in solution. Chemical Society Reviews, 2005. **34**(10): p. 875-900.
7. Langen, P. and F. Hucho, Karl Lohmann and the Discovery of ATP. Angewandte Chemie International Edition, 2008. **47**(10): p. 1824-1827.
8. Manchester, K.L., Free energy ATP hydrolysis and phosphorylation potential. Biochemical Education, 1980. **8**(3): p. 70-72.
9. Achbergerová, L. and J. Nahálka, Polyphosphate - an ancient energy source and active metabolic regulator. Microbial Cell Factories, 2011. **10**(1): p. 63.
10. Wilson, J.E. and A. Chin, Chelation of divalent cations by ATP, studied by titration calorimetry. Analytical biochemistry, 1991. **193**(1): p. 16-19.
11. Sigel, H. and B. Song, Solution structures of nucleotide-metal ion complexes. Isomeric equilibria. Metal ions in biological systems, 1996. **32**: p. 135-135.
12. Starikov, E.B., I. Panas, and B. Nordén, Chemical-to-Mechanical Energy Conversion in Biomacromolecular Machines: A Plasmon and Optimum Control Theory for Directional Work. 1. General Considerations. The Journal of Physical Chemistry B, 2008. **112**(28): p. 8319-8329.
13. George, P., et al., "Squiggle-H2O". An enquiry into the importance of solvation effects in phosphate ester and anhydride reactions. Biochimica et Biophysica Acta (BBA) - Bioenergetics, 1970. **223**(1): p. 1-15.
14. Mildvan, A.S., Role of magnesium and other divalent cations in ATP-utilizing enzymes. Magnesium, 1987. **6**(1): p. 28-33.
15. Shikama, K., Standard free energy maps for the hydrolysis of ATP as a function of pH, pMg and pCa. Archives of Biochemistry and Biophysics, 1971. **147**(1): p. 311-317.
16. Glonek, T., ³¹P NMR of Mg-ATP in dilute solutions: Complexation and exchange. International Journal of Biochemistry, 1992. **24**(10): p. 1533-1559.
17. Alberty, R.A., Enzymes: Units of biological structure and function. Journal of Chemical Education, 1957. **34**(1): p. A33.
18. Sigel, H., Interactions of metal ions with nucleotides and nucleic acids and their constituents. Chemical Society Reviews, 1993. **22**(4): p. 255-267.
19. TRIBOLET, R. and H. SIGEL, Influence of the protonation degree on the self-association properties of adenosine 5'-triphosphate (ATP). European Journal of Biochemistry, 1988. **170**(3): p. 617-626.
20. ACD/ChemSketch. Advanced Chemistry Development, Inc. (ACD Labs): Toronto, ON, Canada.
21. Lightstone, F.C., et al., A first principles molecular dynamics simulation of the hydrated magnesium ion. Chemical Physics Letters, 2001. **343**(5): p. 549-555.
22. Storer, A.C. and A. Cornish-Bowden, Concentration of MgATP²⁻ and other ions in solution. Calculation of the true concentrations of species present in mixtures of associating ions. Biochem J, 1976. **159**(1): p. 1-5.
23. Bock, J.L., et al., ²⁵Mg NMR Studies of magnesium binding to erythrocyte constituents. Journal of Inorganic Biochemistry, 1991. **44**(2): p. 79-87.
24. Molla, G.S., et al., Mechanistic and kinetics elucidation of Mg²⁺/ATP molar ratio effect on glycerol kinase. Molecular Catalysis, 2018. **445**: p. 36-42.
25. Szabó, Z., Multinuclear NMR studies of the interaction of metal ions with adenine-nucleotides. Coordination chemistry reviews, 2008. **252**(21-22): p. 2362-2380.
26. Bishop, E.O., et al., A P-31-Nmr Study of Monomagnesium and Dimagnesium Complexes of Adenosine 5'-Triphosphate and Model Systems. Biochimica Et Biophysica Acta, 1981. **635**(1): p. 63-72.
27. Sari, J.C., et al., Microcalorimetric study of magnesium-adenosine triphosphate ternary complex. Journal of bioenergetics and biomembranes, 1982. **14**(3): p. 171-179.
28. SIGEL, H., Isomeric equilibria in complexes of adenosine 5'-triphosphate with divalent metal ions. European Journal of Biochemistry, 1987. **165**(1): p. 65-72.
29. Frańska, M., et al., Gas-Phase Internal Ribose Residue Loss from Mg-ATP and Mg-ADP Complexes: Experimental and Theoretical Evidence for Phosphate-Mg-Adenine Interaction. Journal of the American Society for Mass Spectrometry, 2022. **33**(8): p. 1474-1479.
30. Matthies, M. and G. Zundel, Hydration and self-association of adenosine triphosphate, adenosine diphosphate, and their 1:1 complexes with magnesium(II) at various pH values: infrared investigations. Journal of the Chemical Society, Perkin Transactions 2, 1977(14): p. 1824-1830.
31. Harrison, C.B. and K. Schulten, Quantum and Classical Dynamics Simulations of ATP Hydrolysis in Solution. Journal of Chemical Theory and Computation, 2012. **8**(7): p. 2328-2335.
32. Akola, J. and R.O. Jones, ATP Hydrolysis in Water - A Density Functional Study. The Journal of Physical Chemistry B, 2003. **107**(42): p. 11774-11783.
33. Wang, C., W. Huang, and J.-L. Liao, QM/MM Investigation of ATP Hydrolysis in Aqueous Solution. The Journal of Physical Chemistry B, 2015. **119**(9): p. 3720-3726.
34. Kamerlin, S. and A. Warshel, On the energetics of ATP hydrolysis in solution. The journal of physical chemistry. B, 2009. **113** 47: p. 15692-8.
35. Weber, J. and A.E. Senior, ATP synthase: what we know about ATP hydrolysis and what we do not know about ATP synthesis. Biochimica et Biophysica Acta (BBA) - Bioenergetics, 2000. **1458**(2): p. 300-309.
36. Liao, J.C., et al., The conformational states of Mg.ATP in water. Eur Biophys J, 2004. **33**(1): p. 29-37.
37. Huang, S.L. and M.D. Tsai, Does the magnesium (II) ion interact with the alpha-phosphate of ATP? An investigation by oxygen-17 nuclear magnetic resonance. Biochemistry, 1982. **21**(5): p. 951-959.
38. Rajendran, T.E. and T. Muthukumarasamy, Thermodynamic calculations of biochemical reaction systems at specified pH, pMg, and change in binding of hydrogen and magnesium ions. Asia-Pacific Journal of Chemical Engineering, 2018. **13**(4): p. e2205.
39. Holm, N., The significance of Mg in prebiotic geochemistry. Geobiology, 2012. **10**: p. 269-79.
40. Admiraal, S.J. and D. Herschlag, Mapping the transition state for ATP hydrolysis: implications for enzymatic catalysis. Chemistry & Biology, 1995. **2**(11): p. 729-739.
41. Seidel, R., B. Winter, and S.E. Bradforth, Valence Electronic Structure of Aqueous Solutions: Insights from Photoelectron Spectroscopy. Annual Review of Physical Chemistry, 2016. **67**(1): p. 283-305.

42. Winter, B. and M. Faubel, Photoemission from Liquid Aqueous Solutions. *Chemical Reviews*, 2006. **106**(4): p. 1176-1211.
43. Ottosson, N., et al., On the Origins of Core-Electron Chemical Shifts of Small Biomolecules in Aqueous Solution: Insights from Photoemission and ab Initio Calculations of Glycineaq. *Journal of the American Chemical Society*, 2011. **133**(9): p. 3120-3130.
44. Nolting, D., et al., pH-Induced Protonation of Lysine in Aqueous Solution Causes Chemical Shifts in X-ray Photoelectron Spectroscopy. *Journal of the American Chemical Society*, 2007. **129**(45): p. 14068-14073.
45. Bruce, J.P. and J.C. Hemminger, Characterization of Fe²⁺ Aqueous Solutions with Liquid Jet X-ray Photoelectron Spectroscopy: Chloride Depletion at the Liquid/Vapor Interface Due to Complexation with Fe²⁺. *The Journal of Physical Chemistry B*, 2019. **123**(39): p. 8285-8290.
46. Malerz, S., et al., Following in Emil Fischer's Footsteps: A Site-Selective Probe of Glucose Acid-Base Chemistry. *The Journal of Physical Chemistry A*, 2021. **125**(32): p. 6881-6892.
47. Schroeder, C.A., et al., Oxidation Half-Reaction of Aqueous Nucleosides and Nucleotides via Photoelectron Spectroscopy Augmented by ab Initio Calculations. *Journal of the American Chemical Society*, 2015. **137**(1): p. 201-209.
48. Mathe, Z., et al., Phosphorus K β X-ray emission spectroscopy detects non-covalent interactions of phosphate biomolecules in situ. *Chemical Science*, 2021. **12**(22): p. 7888-7901.
49. Lanir, A. and N.T. Yu, A Raman spectroscopic study of the interaction of divalent metal ions with adenine moiety of adenosine 5'-triphosphate. *Journal of Biological Chemistry*, 1979. **254**(13): p. 5882-5887.
50. Cohn, M. and T.R. Hughes, Nuclear Magnetic Resonance Spectra of Adenosine Di- and Triphosphate: II. EFFECT OF COMPLEXING WITH DIVALENT METAL IONS. *Journal of Biological Chemistry*, 1962. **237**(1): p. 176-181.
51. McFadden, R.M.L., et al., Magnesium(II)-ATP Complexes in 1-Ethyl-3-Methylimidazolium Acetate Solutions Characterized by ³¹Mg β -Radiation-Detected NMR Spectroscopy. *Angewandte Chemie International Edition*, 2022. **61**(35): p. e202207137.
52. Castellani, M.E., D. Avagliano, and J.R.R. Verlet, Ultrafast Dynamics of the Isolated Adenosine-5'-triphosphate Dianion Probed by Time-Resolved Photoelectron Imaging. *The Journal of Physical Chemistry A*, 2021. **125**(17): p. 3646-3652.
53. Shimada, H., et al., Structural changes of nucleic acid base in aqueous solution as observed in X-ray absorption near edge structure (XANES). *Chemical Physics Letters*, 2014. **591**: p. 137-141.
54. Kelly, D.N., et al., Communication: Near edge x-ray absorption fine structure spectroscopy of aqueous adenosine triphosphate at the carbon and nitrogen K-edges. *The Journal of Chemical Physics*, 2010. **133**(10): p. 101103.
55. Pluhařová, E., et al., Transforming anion instability into stability: contrasting photoionization of three protonation forms of the phosphate ion upon moving into water. *J Phys Chem B*, 2012. **116**(44): p. 13254-64.
56. Seidel, R., S. Thürmer, and B. Winter, Photoelectron Spectroscopy Meets Aqueous Solution: Studies from a Vacuum Liquid Microjet. *The Journal of Physical Chemistry Letters*, 2011. **2**(6): p. 633-641.
57. Ekholm, V., et al., Strong enrichment of atmospherically relevant organic ions at the aqueous interface: the role of ion pairing and cooperative effects. *Physical Chemistry Chemical Physics*, 2018. **20**(42): p. 27185-27191.
58. Aziz, E.F., et al., Interaction between liquid water and hydroxide revealed by core-hole de-excitation. *Nature*, 2008. **455**(7209): p. 89-91.
59. Mudryk, K.D., et al., The electronic structure of the aqueous permanganate ion: aqueous-phase energetics and molecular bonding studied using liquid jet photoelectron spectroscopy. *Physical Chemistry Chemical Physics*, 2020. **22**(36): p. 20311-20330.
60. Jahnke, T., et al., Interatomic and Intermolecular Coulombic Decay. *Chemical Reviews*, 2020. **120**(20): p. 11295-11369.
61. Gopakumar, G., et al., Probing Aqueous Ions with Non-local Auger Relaxation. *Physical Chemistry Chemical Physics*, 2022.
62. Skitnevskaya, A.D., et al., Two-Sided Impact of Water on the Relaxation of Inner-Valence Vacancies of Biologically Relevant Molecules. *The Journal of Physical Chemistry Letters*, 2023: p. 1418-1426.
63. Wang, P., et al., Thermodynamic parameters for the interaction of adenosine 5'-diphosphate, and adenosine 5'-triphosphate with Mg²⁺ from 323.15 to 398.15 K. *Journal of Solution Chemistry*, 1995. **24**(10): p. 989-1012.
64. Viehhaus, J., et al., The Variable Polarization XUV Beamline P04 at PETRA III: Optics, mechanics and their performance. *Nuclear Instruments and Methods in Physics Research Section A: Accelerators, Spectrometers, Detectors and Associated Equipment*, 2013. **710**: p. 151-154.
65. Malerz, S., et al., A setup for studies of photoelectron circular dichroism from chiral molecules in aqueous solution. *Review of Scientific Instruments*, 2022. **93**(1): p. 015101.
66. Winter, B., Liquid microjet for photoelectron spectroscopy. *Nuclear Instruments and Methods in Physics Research Section A: Accelerators, Spectrometers, Detectors and Associated Equipment*, 2009. **601**(1): p. 139-150.
67. Thürmer, S., et al., Accurate Vertical Ionization Energy and Work Function Determinations of Liquid Water and Aqueous Solutions. *Chemical Science*, 2021. **12**(31): p. 10558-10582.
68. Pohl, M.N., et al., Do water's electrons care about electrolytes? *Chemical science*, 2019. **10**(3): p. 848-865.
69. Gilbert, A.T.B., N.A. Besley, and P.M.W. Gill, Self-Consistent Field Calculations of Excited States Using the Maximum Overlap Method (MOM). *The Journal of Physical Chemistry A*, 2008. **112**(50): p. 13164-13171.
70. Epifanovsky, E., et al., Software for the frontiers of quantum chemistry: An overview of developments in the Q-Chem 5 package. *The Journal of Chemical Physics*, 2021. **155**(8): p. 084801.
71. Macetti, G. and A. Genoni, Initial Maximum Overlap Method for Large Systems by the Quantum Mechanics/Extremely Localized Molecular Orbital Embedding Technique. *Journal of Chemical Theory and Computation*, 2021. **17**(7): p. 4169-4182.
72. Mennucci, B. and J. Tomasi, Continuum solvation models: A new approach to the problem of solute's charge distribution and cavity boundaries. *The Journal of Chemical Physics*, 1997. **106**(12): p. 5151-5158.
73. Cancès, E., B. Mennucci, and J. Tomasi, A new integral equation formalism for the polarizable continuum model: Theoretical background and applications to isotropic and anisotropic dielectrics. *The Journal of Chemical Physics*, 1997. **107**(8): p. 3032-3041.
74. Xu, L. and M.L. Coote, Improving the Accuracy of PCM-UAHF and PCM-UAKS Calculations Using Optimized Electrostatic Scaling Factors. *Journal of Chemical Theory and Computation*, 2019. **15**(12): p. 6958-6967.
75. M. J. Frisch, G.W.T., H. B. Schlegel, G. E. Scuseria, M. A. Robb, J. R. Cheeseman, G. Scalmani, V. Barone, B. Mennucci, G. A. Petersson, H. Nakatsuji, M. Caricato, X. Li, H. P. Hratchian, A. F. Izmaylov, J. Bloino, G. Zheng, J. L. Sonnenberg, M. Hada, M. Ehara, K. Toyota, R. Fukuda, J. Hasegawa, M. Ishida, T. Nakajima, Y. Honda, O. Kitao, H. Nakai, T. Vreven, J. A. Montgomery, Jr., J. E. Peralta, F. Ogliaro, M. Bearpark, J. J. Heyd, E. Brothers, K. N. Kudin, V. N.

Staroverov, T. Keith, R. Kobayashi, J. Normand, K. Raghavachari, A. Rendell, J. C. Burant, S. S. Iyengar, J. Tomasi, M. Cossi, N. Rega, J. M. Millam, M. Klene, J. E. Knox, J. B. Cross, V. Bakken, C. Adamo, J. Jaramillo, R. Gomperts, R. E. Stratmann, O. Yazyev, A. J. Austin, R. Cammi, C. Pomelli, J. W. Ochterski, R. L. Martin, K. Morokuma, V. G. Zakrzewski, G. A. Voth, P. Salvador, J. J. Dannenberg, S. Dapprich, A. D. Daniels, O. Farkas, J. B. Foresman, J. V. Ortiz, J. Cioslowski, and D. J. Fox, Gaussian 09, Revision D.01. 2013, Gaussian Inc.: Wallingford CT.

76. Winter, B., et al., Full Valence Band Photoemission from Liquid Water Using EUV Synchrotron Radiation. *The Journal of Physical Chemistry A*, 2004. **108**(14): p. 2625-2632.

77. Winter, B. and M. Faubel, Photoemission from liquid aqueous solutions. *Chem Rev*, 2006. **106**(4): p. 1176-211.

78. Trofimov, A.B., et al., Photoelectron spectra of the nucleobases cytosine, thymine and adenine. *Journal of Physics B: Atomic, Molecular and Optical Physics*, 2006. **39**(2): p. 305.

79. Sherwood, P.M.A., Introduction to Studies of Phosphorus-Oxygen Compounds by XPS. *Surface Science Spectra*, 2002. **9**(1): p. 62-66.

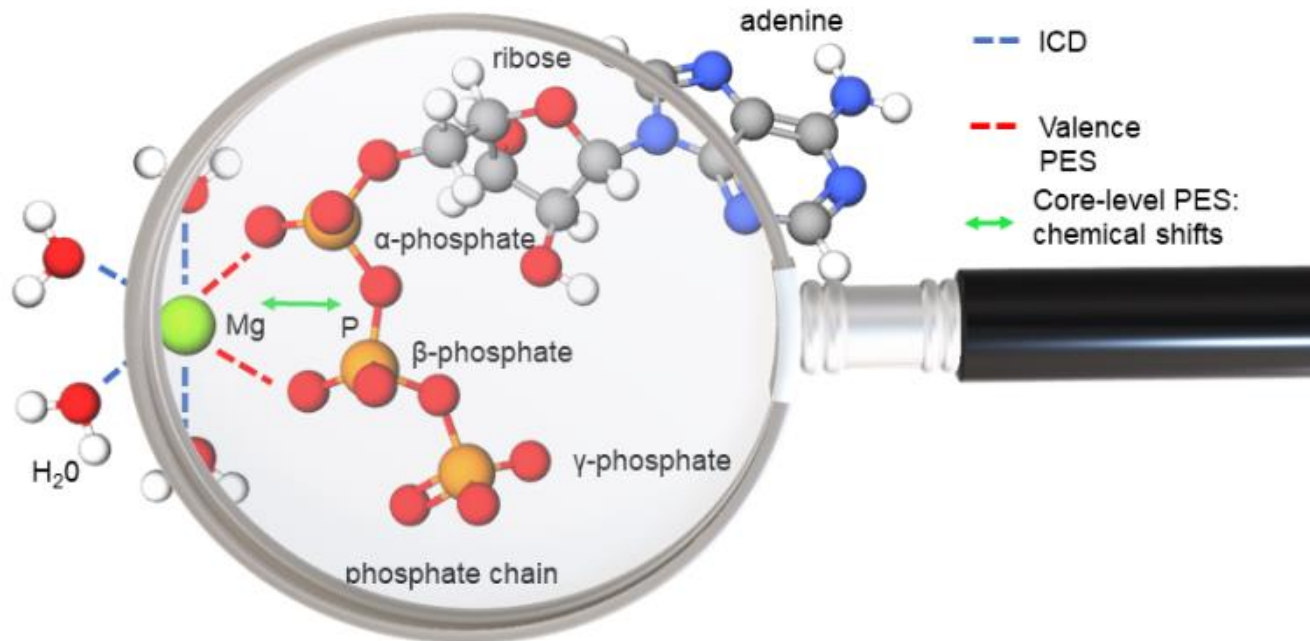
80. Credidio, B., et al., Quantitative electronic structure and work-function changes of liquid water induced by solute. *Physical Chemistry Chemical Physics*, 2022. **24**(3): p. 1310-1325.

81. Xiao, C.-Q., et al., Binding thermodynamics of divalent metal ions to several biological buffers. *Thermochimica Acta*, 2020. **691**: p. 178721.

82. Sigel, H., et al., Comparison of the stabilities of monomeric metal ion complexes formed with adenosine 5'-triphosphate (ATP) and pyrimidine-nucleoside 5'-triphosphate (CTP, UTP, TTP) and evaluation of the isomeric equilibria in the complexes of ATP and CTP. *Inorganic Chemistry*, 1987. **26**(13): p. 2149-2157.

83. Sigel, H., Metal ion-assisted stacking interactions and the facilitated hydrolysis of nucleoside 5'-triphosphates. *Pure and Applied Chemistry*, 1998. **70**(4): p. 969-976.

84. Rizkalla, E.N., M.S. Antonious, and S.S. Anis, X-ray photoelectron and potentiometric studies of some calcium complexes. *Inorganica Chimica Acta*, 1985. **96**(2): p. 171-178.



Supporting Information

How does $\text{Mg}^{2+}_{(\text{aq})}$ interact with $\text{ATP}_{(\text{aq})}$? Observations through the lens of liquid-jet photoelectron spectroscopy

Karen Mudryk^{1,#}, Chin Lee^{1,2,3,a,#}, Lukáš Tomaník^{4,#}, Sebastian Malerz¹, Florian Trinter^{1,5}, Uwe Hergenhahn¹, Daniel M. Neumark^{2,3}, Petr Slavíček⁴, Stephen Bradforth^{6,*} and Bernd Winter^{1,*}

¹Molecular Physics, Fritz-Haber-Institut der Max-Planck-Gesellschaft, Faradayweg 4-6, 14195 Berlin, Germany

²Department of Chemistry, University of California, Berkeley, CA 94720, USA

³Chemical Sciences Division, Lawrence Berkeley National Laboratory, Berkeley, CA 94720, USA

⁴Department of Physical Chemistry, University of Chemistry and Technology, Technická 5, Prague 6 16628, Czech Republic

⁵Institut für Kernphysik, Goethe-Universität, Max-von-Laue-Straße 1, 60438 Frankfurt am Main, Germany

⁶Department of Chemistry, University of Southern California, Los Angeles, CA 90089, USA

Current addresses:

^aSandia National Laboratories California, Livermore, CA 94550, USA

[#]Authors contributed equally

*Corresponding authors: stephen.bradforth@usc.edu, winter@fhi-berlin.mpg.de

Table of contents

Sample preparation	3
Possible ‘open form’ and ‘closed form’ configuration of $\text{Mg}_2\text{ATP}_{(\text{aq})}$	3
Predicted composition of the $\text{ATP}_{(\text{aq})}$ samples with dissolved Mg^{2+} as a function of the $\text{Mg}^{2+}/\text{ATP}$ concentration ratio	3
Photoelectron spectra from $\text{Tris}_{(\text{aq})}$ solutions with and without dissolved Mg^{2+}	5
Valence photoelectron spectra of $\text{ATP}_{(\text{aq})}$, $\text{ADP}_{(\text{aq})}$, and $\text{AMP}_{(\text{aq})}$	6
Valence photoelectron spectra of $\text{ADP}_{(\text{aq})}$ with $\text{Mg}^{2+}_{(\text{aq})}$	7
Linear baselines to the P 2s data presented in Figure 3(e) in the main text	7
Data treatment to determine α -, β -, and γ -phosphate P 2s binding energies in $\text{ATP}_{(\text{aq})}$	8
Intermolecular Coulombic decay (ICD) spectra of $\text{ATP}_{(\text{aq})}$ solutions with dissolved Mg^{2+}	9
Sample input for calculations of P 2s binding energies using Q-Chem, version 6.0	10
Cartesian coordinates of the structures used to calculate P 2s binding energies	14
Cartesian coordinates of the structures used to calculate Mg 2s and 2p binding energies	25
References	30

Sample preparation

Table S1. Concentration of $\text{Mg}(\text{NO}_3)_{2(\text{aq})}$ and $\text{Tris}_{(\text{aq})}$ (tris(hydroxymethyl)aminomethane) in the $\text{ATP}_{(\text{aq})}$, $\text{ADP}_{(\text{aq})}$, and $\text{AMP}_{(\text{aq})}$ solutions used in this work. The solution pH was 8.2 in all samples. All values are in mol dm^{-3} .

$\text{Mg}^{2+}/\text{ATP}$ ratio	$\text{Mg}(\text{NO}_3)_{2(\text{aq})}$	$\text{Tris}_{(\text{aq})}$		
		0.5 M $\text{ATP}_{(\text{aq})}$	0.5 M $\text{ADP}_{(\text{aq})}$	0.5 M $\text{AMP}_{(\text{aq})}$
0	0	1.16	1.36	0.23
0.25	0.125	1.21	1.52	
0.5	0.25	1.32	1.70	
0.75	0.375	1.43	1.77	
1	0.5	1.54	1.93	
1.5	0.75	1.65	2.34	

Possible ‘open form’ and ‘closed form’ configuration of $\text{Mg}_2\text{ATP}_{(\text{aq})}$

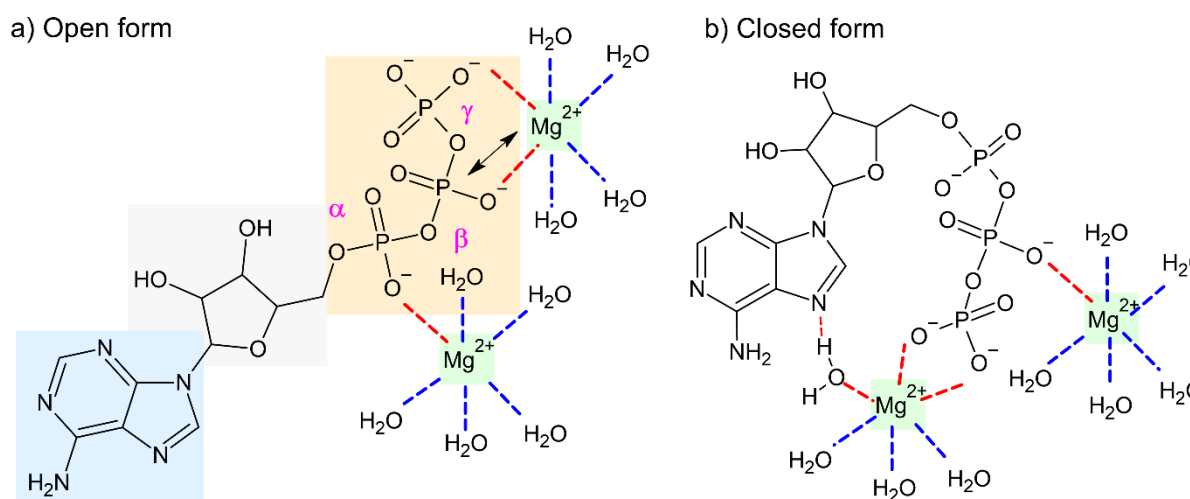


Figure S1. Possible molecular structures adopted by $\text{Mg}_2\text{ATP}_{(\text{aq})}$. (a) Open form. (b) Closed form. This figure was produced using the ACD / ChemSketch software [1].

Predicted composition of the $\text{ATP}_{(\text{aq})}$ samples with dissolved Mg^{2+} as a function of the $\text{Mg}^{2+}/\text{ATP}$ concentration ratio

The composition of the $\text{ATP}_{(\text{aq})}$ samples with dissolved Mg^{2+} was calculated as follows. First, we assumed the species in solution to be ATP^{4-} , HATP^{3-} , $\text{H}_2\text{ATP}^{2-}$, MgATP^{2-} , Mg_2ATP , MgHATP^- , MgH_2ATP , Mg^{2+} , Na^+ , H^+ , and OH^- , with a solution pH of 8.2 to match the experimental conditions. Thus,

$$[\text{H}^+] = 10^{-8.2} \quad (1)$$

We used equilibrium constants from Storer and Cornish-Bowden [2] – namely, Equations (1), (2), (4), (5), (6), and (7) from Table 2. Notably, the values correspond to solutions of lower ionic strength than those studied here. Nevertheless, they still serve to allow for a qualitative estimate of our system.

$$\frac{[\text{H}_2\text{ATP}^{2-}]}{[\text{H}^+] \cdot [\text{HATP}^{3-}]} = 8.5 \cdot 10^3 \quad (2)$$

$$\frac{[\text{HATP}^{3-}]}{[\text{H}^+] \cdot [\text{ATP}^{4-}]} = 1.09 \cdot 10^7 \quad (3)$$

$$\frac{[\text{MgH}_2\text{ATP}]}{[\text{Mg}^{2+}] \cdot [\text{H}_2\text{ATP}^{2-}]} = 2.0 \cdot 10^1 \quad (4)$$

$$\frac{[\text{MgHATP}^-]}{[\text{Mg}^{2+}] \cdot [\text{HATP}^{3-}]} = 5.42 \cdot 10^2 \quad (5)$$

$$\frac{[\text{MgATP}^{2-}]}{[\text{Mg}^{2+}] \cdot [\text{ATP}^{4-}]} = 3.48 \cdot 10^4 \quad (6)$$

$$\frac{[\text{Mg}_2\text{ATP}]}{[\text{Mg}^{2+}] \cdot [\text{MgATP}^{2-}]} = 4.0 \cdot 10^1 \quad (7)$$

In addition, we used equations for mass balance, where $c_0(\text{Na}_2\text{H}_2\text{ATP})$ is the initial concentration of the ATP compound and $c_0(\text{Mg}(\text{NO}_3)_2)$ is the initial concentration of the Mg salt.

$$c_0(\text{Na}_2\text{H}_2\text{ATP}) = [\text{ATP}^{4-}] + [\text{HATP}^{3-}] + [\text{H}_2\text{ATP}^{2-}] + [\text{MgATP}^{2-}] + [\text{Mg}_2\text{ATP}] + [\text{MgHATP}^-] + [\text{MgH}_2\text{ATP}] \quad (8)$$

$$c_0(\text{Mg}(\text{NO}_3)_2) = [\text{Mg}^{2+}] + [\text{MgATP}^{2-}] + 2 \cdot [\text{Mg}_2\text{ATP}] + [\text{MgHATP}^-] + [\text{MgH}_2\text{ATP}] \quad (9)$$

$$[\text{Na}^+] = 2 \cdot c_0(\text{Na}_2\text{H}_2\text{ATP}) \quad (10)$$

Finally, we considered the self-ionization of water at 25 °C.

$$[\text{H}^+] \cdot [\text{OH}^-] = 10^{-14} \quad (11)$$

This represents a system of 11 equations with 11 unknowns, which was solved for different $\text{Mg}^{2+}/\text{ATP}$ concentration ratios using the Maple 2016 software [3]. The results are reported in Table S2.

Table S2. Calculated concentration of species as a function of $\text{Mg}^{2+}/\text{ATP}$ concentration ratio at a solution pH of 8.2. The values were determined as described in the text, using equilibrium constants from Reference [2]. The total concentration of $\text{ATP}_{(\text{aq})}$ was kept at 0.5 mol dm^{-3} while the total concentration of $\text{Mg}^{2+}_{(\text{aq})}$ was varied in the range $0.125\text{-}0.75 \text{ mol dm}^{-3}$. All values are in mol dm^{-3} .

	0.25:1 ratio	0.5:1 ratio	0.75:1 ratio	1:1 ratio	1.5:1 ratio
$\text{ATP}^{4-}_{(\text{aq})}$	3.51E-01	2.34E-01	1.18E-01	1.57E-02	3.66E-04
$\text{H}^+_{(\text{aq})}$	6.31E-09	6.31E-09	6.31E-09	6.31E-09	6.31E-09
$[\text{H}_2\text{ATP}]^{2-}_{(\text{aq})}$	1.29E-06	8.64E-07	4.36E-07	5.80E-08	1.35E-09
$[\text{HATP}]^{3-}_{(\text{aq})}$	2.41E-02	1.61E-02	8.14E-03	1.08E-03	2.52E-05
$\text{Mg}^{2+}_{(\text{aq})}$	1.02E-05	3.06E-05	9.03E-05	8.54E-04	2.12E-02
$\text{Mg}_2\text{ATP}_{(\text{aq})}$	5.10E-05	3.04E-04	1.34E-03	1.59E-02	2.29E-01
$[\text{MgATP}]^{2-}_{(\text{aq})}$	1.25E-01	2.49E-01	3.72E-01	4.67E-01	2.70E-01
$\text{MgH}_2\text{ATP}_{(\text{aq})}$	2.64E-10	5.28E-10	7.88E-10	9.89E-10	5.73E-10
$[\text{MgHATP}]^{-}_{(\text{aq})}$	1.34E-04	2.67E-04	3.98E-04	5.00E-04	2.89E-04
$\text{OH}^{-}_{(\text{aq})}$	1.58E-06	1.58E-06	1.58E-06	1.58E-06	1.58E-06

Photoelectron spectra from $\text{Tris}_{(\text{aq})}$ solutions with and without dissolved Mg^{2+}

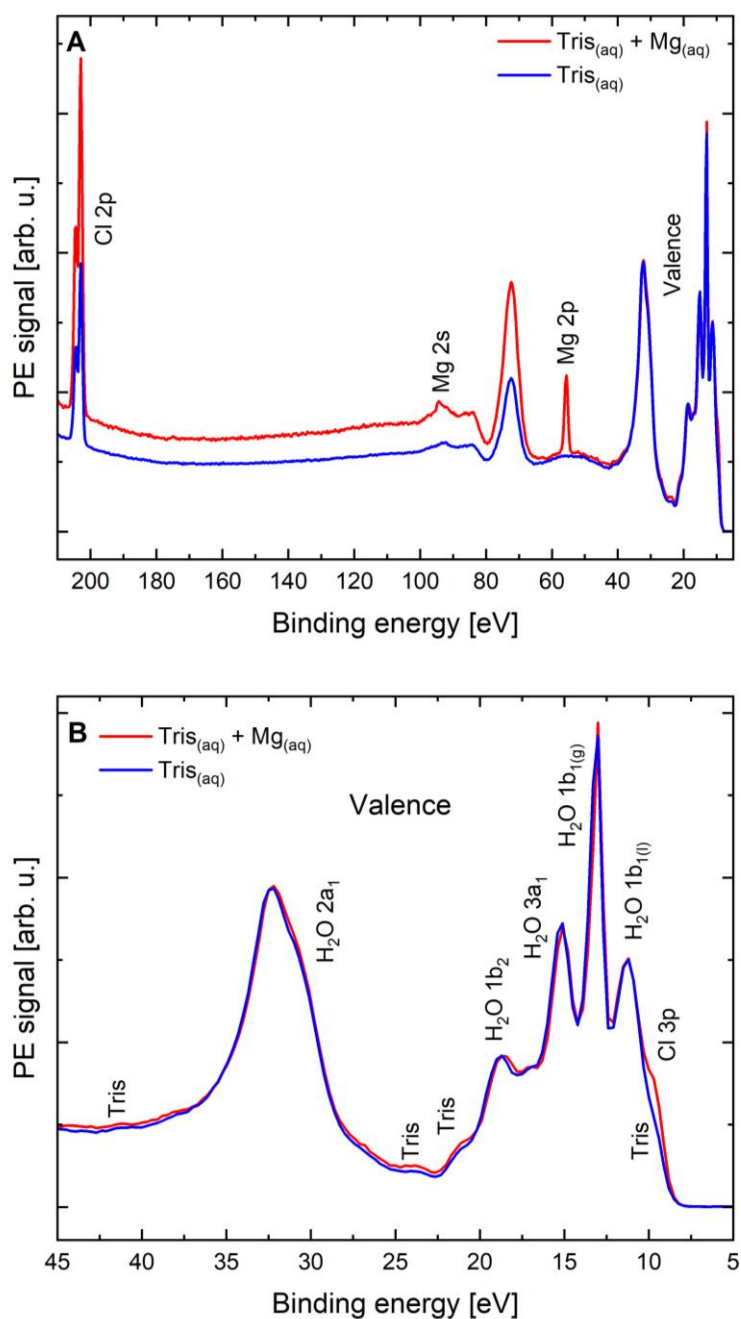


Figure S2. (a) Photoelectron spectra recorded from 3.2 M $\text{Tris}_{(\text{aq})}$ without $\text{Mg}^{2+}_{(\text{aq})}$ (blue line) and with 0.5 M $\text{MgCl}_{2(\text{aq})}$ (red line) using a photon energy of 250 eV. The sample pH was adjusted to 8.2 by addition of concentrated HCl in both cases. The binding energy (BE) scale was calibrated based on the liquid-water solvent valence $1b_1$ peak position, and spectral intensities are displayed to yield its same height. (b) Highlight of the valence spectral region from panel (a). Photoelectron signatures of water and $\text{Cl}_{(\text{aq})}$ are labelled according to References [4] and [5], respectively.

Valence photoelectron spectra of $\text{ATP}_{(\text{aq})}$, $\text{ADP}_{(\text{aq})}$, and $\text{AMP}_{(\text{aq})}$

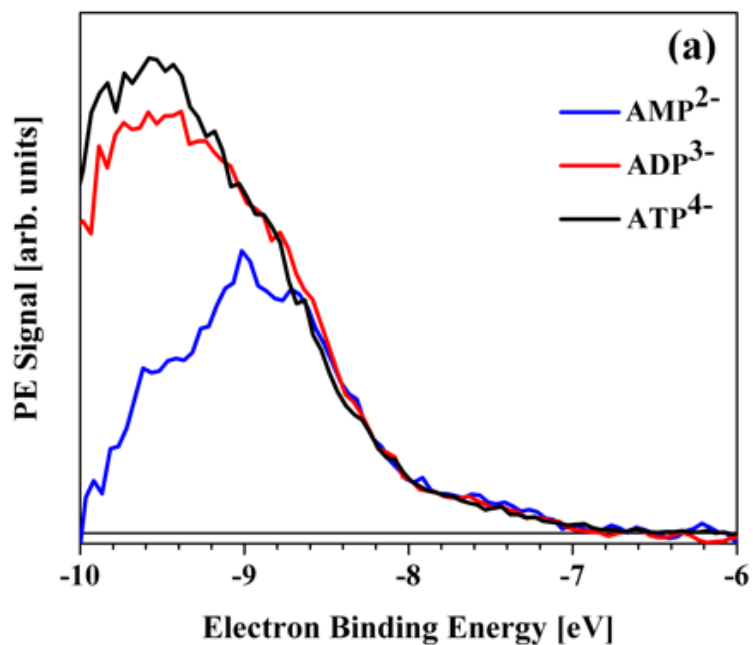


Figure S3. Valence photoelectron signals from $\text{AMP}_{(\text{aq})}$, $\text{ADP}_{(\text{aq})}$, and $\text{ATP}_{(\text{aq})}$ solutions without dissolved Mg^{2+} isolated by subtracting the solvent water contributions, facilitating the identification of the phosphate feature and its changes in signal intensity across the nucleotide series. The figure was extracted from Reference [6]. The experimental conditions used are described in Reference [7].

Valence photoelectron spectra of ADP_(aq) with Mg²⁺_(aq)

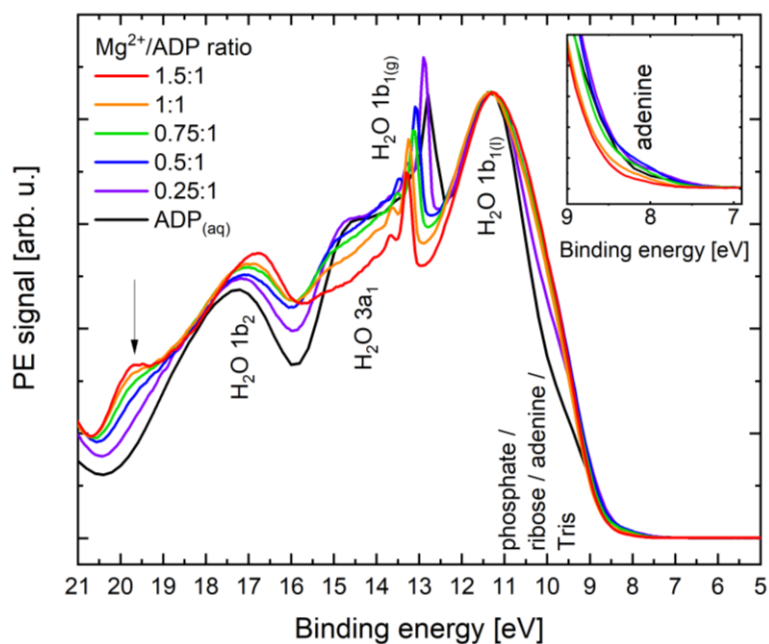


Figure S4. Valence and core-level (Mg 2p, Mg 2s, P 2p, and P 2s) photoelectron spectra from 0.5 M ADP_(aq) samples containing Mg²⁺_(aq) as a function of the Mg²⁺/ADP concentration ratio recorded using a photon energy of 250 eV. The sample pH was 8.2, adjusted by addition of Tris. The BE scale was calibrated based on the liquid-water solvent valence 1b₁ peak position, and spectral intensities are displayed to yield its same height. The figure inset highlights chemical shifts for the adenine unit, hinting to the presence of phosphate–Mg²⁺–adenine interactions, as reported in Reference [8]. The arrow highlights PE signatures due to Mg²⁺–phosphate interactions, as explained in the main text in connection with Figure 3(a).

Linear baselines to the P 2s data presented in Figure 3(e) in the main text

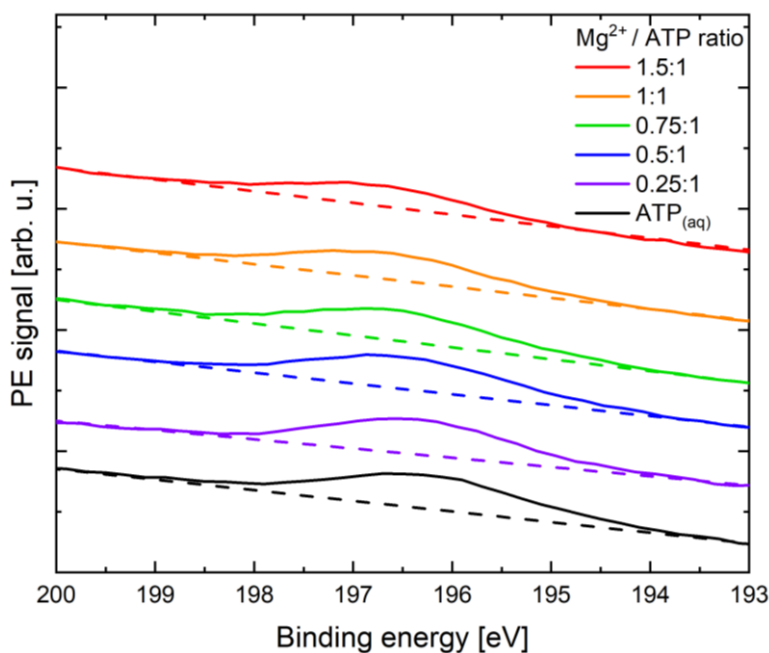


Figure S5. Linear baselines subtracted to the data presented in Figure 3(e) in the main text. The data are shown with a vertical offset for a better comparison.

Data treatment to determine α -, β -, and γ -phosphate P 2s binding energies in ATP_(aq)

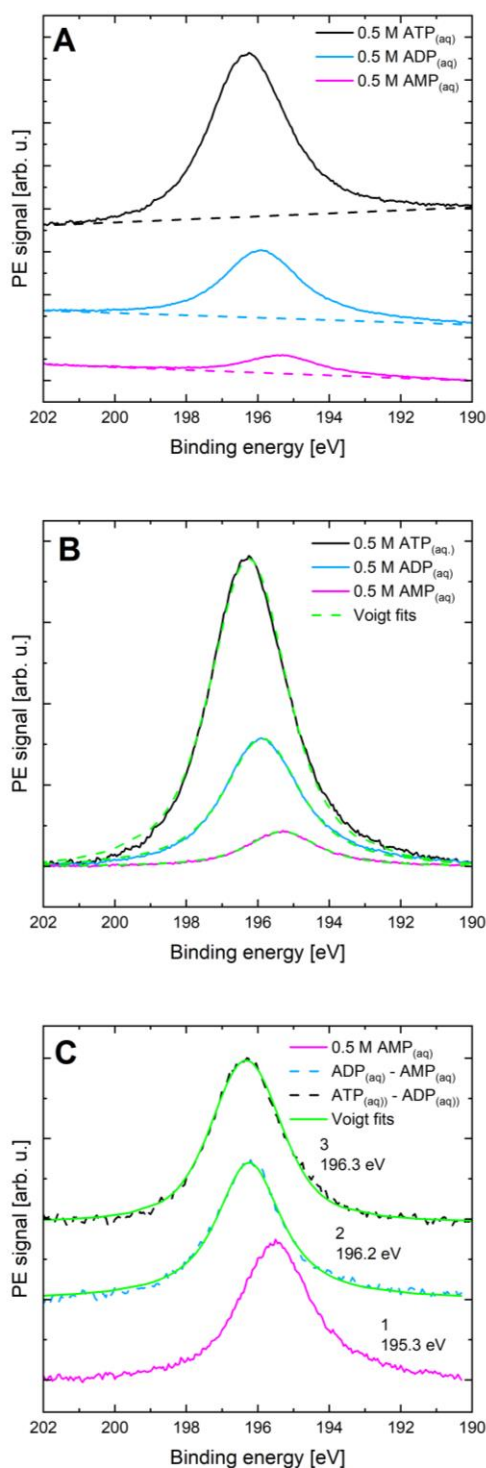


Figure S6. (a) Linear baselines fit to and subtracted from the P 2s AMP_(aq), ADP_(aq), and ATP_(aq) spectra. (b) Voigt fits to the background-subtracted data performed to extract peak areas to re-scale each spectrum based on the number of phosphate units in each sample, as explained in the main text. (c) Voigt fits to the AMP_(aq) and the ADP_(aq)-AMP_(aq) and ATP_(aq)-ADP_(aq) difference spectra. The data are shown with a vertical offset for a better comparison. Peaks 1, 2, and 3 correspond to γ -, β -, and α -phosphate, as described in the main text.

Intermolecular Coulombic decay (ICD) spectra of ATP_(aq) solutions with dissolved Mg²⁺

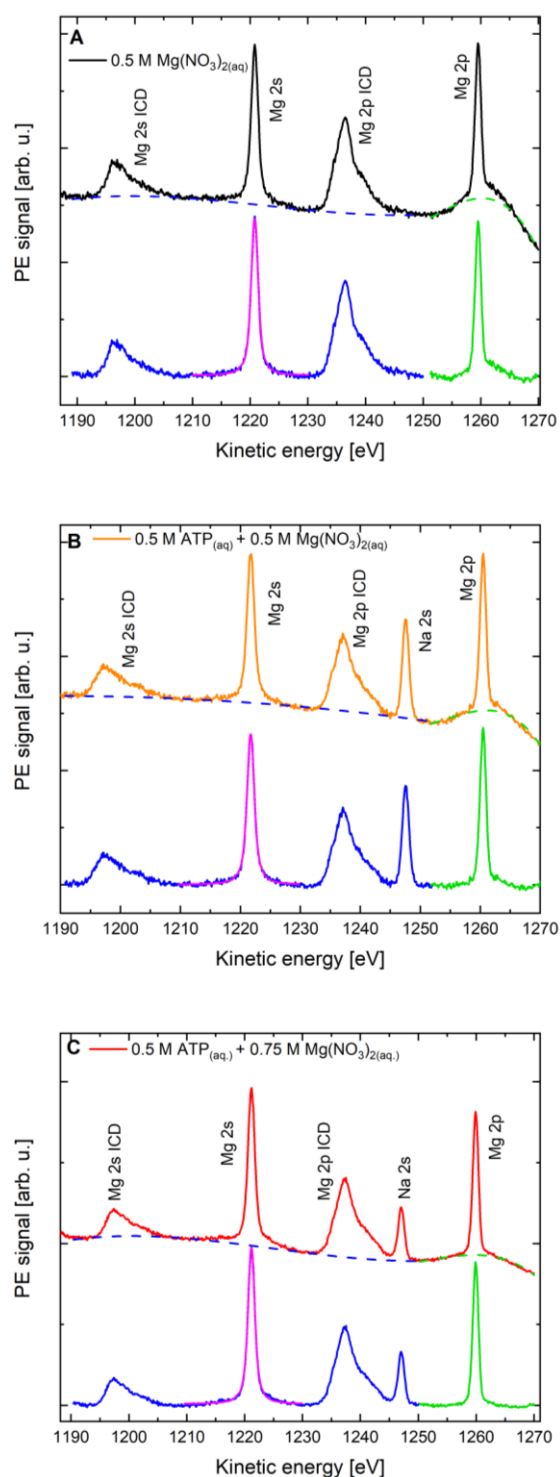


Figure S7. ICD spectra from a 0.5 M Mg(NO₃)_{2(aq)} solution [panel (a)] and samples additionally containing ATP_(aq) at 1:1 and 1.5:1 Mg²⁺/ATP concentration ratios [panels (b) and (c), respectively]. Cubic baselines were fit to and subtracted from different spectral regions – highlighted by green and blue dashed lines – to obtain the background-free data shown at the bottom of each plot and in Figure 6 in the main text (the use of a single baseline per spectrum did not allow the background to be removed completely, particularly in the vicinity of the Mg 2p peak). Voigt profile fits to the Mg 2s feature used to extract peak areas to normalize the signal intensity according to the Mg²⁺_(aq) concentration are shown in magenta.

Sample input for calculations of P 2s binding energies using Q-Chem, version 6.0

\$molecule

-2 1

C	7.224927	-0.822676	1.178578
C	6.400689	0.390773	1.648327
O	5.741657	0.889906	0.512408
C	6.357295	0.400165	-0.665258
C	6.764706	-1.015146	-0.271981
N	5.429865	0.126595	2.680502
C	4.426729	-0.802826	2.709145
C	3.760179	-0.587106	3.893105
N	4.331220	0.463841	4.589294
C	5.297970	0.850033	3.838275
N	4.132054	-1.736044	1.805532
C	3.098102	-2.463627	2.163904
N	2.364894	-2.366194	3.267622
C	2.673168	-1.429240	4.163609
N	1.957320	-1.353158	5.298273
C	5.383016	0.475700	-1.817277
O	5.034723	1.825785	-2.085047
P	5.533519	2.671333	-3.330859
O	7.086128	2.959546	-2.998166
P	7.796586	4.068300	-2.077932
O	9.114600	3.311294	-1.667383
P	10.678216	3.215316	-2.178902
O	10.922827	4.458632	-3.017769
O	7.777934	-1.506934	-1.105013
O	8.578676	-0.448645	1.231810
O	4.774182	3.950285	-3.325847
O	5.528548	1.824879	-4.556795
O	8.111996	5.247946	-2.943544
O	6.986746	4.312065	-0.857579
O	11.454269	3.203851	-0.883496
O	10.774878	1.951695	-2.989088
O	7.892952	3.910242	1.866903
O	8.886263	6.585860	1.873713
O	4.444713	3.630963	0.526843
O	6.631657	7.046811	-0.114316
O	2.995563	0.236236	-4.751444
O	7.395943	-1.171897	-7.894599
O	7.824774	0.477340	-5.580742
O	4.831772	2.698903	-7.194269
O	2.431757	3.795051	-1.615895
O	4.636346	6.771471	-2.335407
O	1.385435	1.259172	-2.503023
O	4.035588	5.163317	-5.855433
O	12.966150	4.476538	-5.001197
O	14.234390	4.236107	-1.054033
O	13.102625	0.908295	-0.257338
O	10.128784	2.142256	1.496512
O	11.223501	5.922243	0.264295
O	13.307154	0.620968	-3.152611
O	9.350816	-0.462957	-3.353000
O	10.034819	2.394841	-5.715182
O	15.023858	2.932689	-3.590595
O	10.321438	7.235626	-2.025491
O	6.733315	6.081292	-5.374094
O	9.472906	5.150173	-5.608173
Mg	9.851872	6.021003	-3.696028

H	2.801346	-3.237732	1.480314
H	2.035870	-0.538121	5.866455
H	1.088072	-1.840026	5.337770
H	5.967154	1.657172	4.057903
H	7.068832	1.137048	2.046875
H	7.057422	-1.696537	1.791669
H	9.083442	-1.045094	0.688867
H	5.903130	-1.666458	-0.293672
H	7.705345	-2.449706	-1.196279
H	7.241875	0.986102	-0.886453
H	5.815846	0.010135	-2.691753
H	4.465763	-0.036247	-1.564339
H	0.468714	1.380529	-2.720858
H	3.103148	3.902189	-2.288935
H	4.740231	5.856743	-2.593883
H	4.110315	4.771779	-4.985102
H	3.820253	0.716911	-4.739126
H	5.122023	2.366727	-6.342873
H	7.053876	0.926309	-5.228815
H	6.666984	-1.751152	-7.707936
H	6.785323	6.124739	-0.322195
H	5.173605	3.989064	0.023919
H	7.563655	3.969013	0.970381
H	8.535770	5.702781	2.004410
H	13.327405	3.942895	-0.983119
H	11.243794	4.997076	0.018199
H	10.514336	2.459124	0.678530
H	12.526669	1.657321	-0.424827
H	14.536007	2.115559	-3.482834
H	12.451211	1.046945	-3.232718
H	9.814979	0.346478	-3.128514
H	10.344013	2.228645	-4.821276
H	10.657318	6.801758	-1.232143
H	12.299761	4.271847	-4.340567
H	6.796653	5.660194	-4.519793
H	8.570916	5.300176	-5.884832
H	2.481603	0.582441	-4.023542
H	7.518432	-0.640673	-7.106659
H	5.614821	2.787914	-7.724618
H	8.259211	0.066565	-4.830605
H	4.197890	4.439183	-6.458247
H	4.757724	7.277308	-3.130167
H	2.937496	3.704587	-0.808888
H	1.692518	2.102843	-2.164560
H	4.659113	2.704974	0.598189
H	8.656785	3.335200	1.816173
H	8.258972	7.017199	1.299901
H	5.957097	7.303932	-0.737174
H	10.476687	6.050143	0.849382
H	9.690837	1.319313	1.296189
H	12.578179	0.273310	0.215853
H	14.571194	3.829778	-1.850518
H	13.410962	0.503367	-2.210164
H	14.479139	3.473358	-4.159442
H	8.845222	-0.714022	-2.584581
H	9.265208	1.836569	-5.818751
H	9.666441	7.863729	-1.741839
H	12.703440	4.018541	-5.791878
H	5.841635	5.917281	-5.682034
H	9.630392	4.202328	-5.678875

O 11.583857 6.941532 -4.587323
H 12.055758 7.491578 -3.970534
H 12.216189 6.299676 -4.913845
O 8.753769 7.733178 -4.382556
H 9.228149 8.347153 -4.933370
H 7.950080 7.504803 -4.851660
\$end

\$rem
METHOD HF
BASIS General
THRESH 12
MAX_SCF_CYCLES 129
solvent_method pcm
PCM_PRINT 1
MEM_TOTAL 384000
MEM_STATIC 2000
\$end

\$basis
H 0
aug-cc-pVTZ

C 0
aug-cc-pVTZ

O 0
aug-cc-pVTZ

N 0
aug-cc-pVTZ

P 0
aug-cc-pCVTZ

Mg 0
aug-cc-pVTZ

\$end

\$pcm
THEORY IEFPCM
RADII Bondi
vdwScale 1.2
NonEquilibrium
\$end

\$solvent
Dielectric 78.39
OpticalDielectric 1.78
\$end

@@@
\$molecule
-1 2
READ
\$end
\$rem
METHOD HF
BASIS General

THRESH 12
MAX_SCF_CYCLES 129
unrestricted TRUE
mom_start 1
MOM_METHOD IMOM
scf_guess read
solvent_method pcm
PCM_PRINT 1
MEM_TOTAL 384000
MEM_STATIC 2000
\$end

\$basis
H 0
aug-cc-pVTZ

C 0
aug-cc-pVTZ

O 0
aug-cc-pVTZ

N 0
aug-cc-pVTZ

P 0
aug-cc-pCVTZ

Mg 0
aug-cc-pVTZ

\$end

\$pcm
THEORY IEFPCM
RADII Bondi
vdwScale 1.2
StateSpecific Marcus
\$end

\$solvent
Dielectric 78.39
OpticalDielectric 1.78
\$end

\$occupied
1:265
1:58 60:265
\$end

Cartesian coordinates of the structures used to calculate P 2s binding energies

Na-ATP³⁻

C	2.562342	-3.449378	2.664820
C	3.204769	-2.227700	2.906797
C	4.242229	-1.900484	2.064503
N	4.687673	-2.638824	1.049400
C	4.013198	-3.758967	0.918551
N	2.995601	-4.198189	1.651377
N	3.012077	-1.234098	3.850704
C	3.905221	-0.355822	3.569666
N	4.698950	-0.687927	2.501922
C	5.742018	0.142776	1.953722
C	7.114733	-0.533621	1.782152
C	7.310280	-0.547873	0.257979
C	6.456150	0.629086	-0.202557
O	5.350532	0.596021	0.684694
O	8.042435	0.292037	2.429827
C	5.952404	0.508860	-1.623004
O	5.165330	1.638281	-1.969054
P	5.618716	2.734025	-3.027027
O	6.123016	2.079384	-4.267003
O	8.646604	-0.388294	-0.144361
N	1.558101	-3.909577	3.430522
O	6.830785	3.406831	-2.220814
P	8.041020	4.417642	-2.525158
O	8.184963	5.264320	-1.306155
O	4.494159	3.701511	-3.153608
O	9.230349	3.370919	-2.628099
P	10.865007	3.565300	-2.768880
O	11.298252	2.275451	-3.441686
O	7.827742	5.092877	-3.834313
O	11.055382	4.805637	-3.612283
O	11.388685	3.692461	-1.358655
O	3.269612	2.764488	0.833269
O	4.080978	6.498259	-2.566019
O	2.061613	2.998321	-1.805741
O	3.869324	4.697277	-5.817598
O	4.990345	4.960832	1.612794
O	5.891373	6.872813	-0.376894
O	9.867224	7.454267	-0.507046
O	7.759914	4.195377	1.392843
O	1.849858	0.416182	-3.067317
O	3.975747	0.060522	-5.075832
O	8.035304	0.175732	-5.248324
O	5.889638	2.946088	-6.976238
O	10.357737	3.504718	2.517755
O	11.587875	5.491397	0.824728
O	10.975305	1.539212	0.415755
O	14.219562	3.265406	-0.986288
O	12.994398	0.603172	-1.616928
O	9.792412	-0.144778	-3.000530
O	10.267252	1.835167	-6.109671
O	13.708199	2.094122	-4.983940
O	13.102261	4.882776	-5.608349
O	11.878843	7.260327	-2.619139

O	5.793276	6.710287	-4.967204
O	10.567024	4.532141	-7.024065
Na	9.561578	5.772256	-5.235461
O	8.073131	7.065658	-6.667463
O	10.702070	7.883720	-5.140986
H	4.317315	-4.406836	0.117080
H	1.087350	-3.278851	4.042024
H	1.021970	-4.676925	3.087027
H	4.054152	0.564733	4.096933
H	5.850971	0.977798	2.628245
H	7.135054	-1.527615	2.206566
H	8.923621	-0.015100	2.254294
H	6.909432	-1.469322	-0.141254
H	9.096601	-1.225275	-0.100945
H	7.001850	1.556031	-0.074696
H	6.788997	0.403572	-2.298168
H	5.316944	-0.359973	-1.718520
H	2.829752	3.286257	-2.300272
H	3.894263	2.052696	0.720867
H	4.159711	5.548354	-2.657735
H	3.944014	4.315850	-4.942537
H	0.985534	0.344576	-3.455060
H	6.053875	2.646172	-6.080282
H	7.381366	0.792126	-4.920327
H	4.679578	0.672124	-4.875300
H	6.657491	6.386287	-0.680416
H	5.132011	5.649946	0.963307
H	7.977039	4.497753	0.511140
H	9.273546	6.762660	-0.802164
H	13.303992	3.525988	-1.096758
H	11.541161	4.922107	0.052788
H	10.807361	4.235401	2.090927
H	11.042267	2.274407	-0.202917
H	12.930400	2.117679	-4.421028
H	12.481570	1.105077	-2.249749
H	10.264716	0.685023	-3.095547
H	10.617277	1.978689	-5.228242
H	11.683045	6.346679	-2.859671
H	12.498846	4.917237	-4.863015
H	6.409374	6.133821	-4.507732
H	10.376916	3.610955	-6.841874
H	1.868867	1.261945	-2.614331
H	3.304525	0.204729	-4.410383
H	6.658031	3.442552	-7.232684
H	8.560619	-0.059322	-4.483290
H	4.426639	4.151224	-6.369643
H	4.558485	6.843895	-3.316749
H	3.797415	3.531122	1.061364
H	2.373390	2.914709	-0.904207
H	5.860052	4.581654	1.731264
H	8.583570	3.938947	1.805305
H	10.518287	7.539224	-1.201386
H	5.259320	6.823753	-1.094568
H	11.022941	6.231107	0.609074
H	10.562939	2.744727	1.975235
H	10.166763	1.080442	0.206364

H	14.200422	2.325205	-1.139131
H	12.471971	0.631874	-0.819744
H	14.447776	1.947394	-4.406081
H	9.372651	-0.116589	-2.146644
H	9.465173	1.329738	-5.982723
H	12.792465	7.286836	-2.359715
H	13.490784	4.011574	-5.556513
H	5.164334	6.126723	-5.391907
H	11.488068	4.641375	-6.791937
H	11.242137	7.885667	-4.351083
H	11.273935	8.145343	-5.853284
H	8.434902	7.942655	-6.612911
H	7.227414	7.101730	-6.220426

[Mg-ATP]²⁻ (Mg²⁺ bound to α -, β -, and γ -phosphate)

C	0.954635	-3.123957	3.443092
C	1.610854	-1.889433	3.533673
C	2.789449	-1.766177	2.834651
N	3.356160	-2.711252	2.086101
C	2.654092	-3.822032	2.074538
N	1.508199	-4.078531	2.695855
N	1.315758	-0.714236	4.201936
C	2.287604	0.072025	3.904475
N	3.229610	-0.495530	3.083724
C	4.391895	0.185018	2.568644
O	4.242835	0.366270	1.182247
C	5.473575	0.158313	0.513960
C	6.155354	-0.917085	1.351917
C	5.737815	-0.535146	2.777581
O	6.619309	0.403858	3.330351
O	7.543763	-0.887231	1.156396
C	5.220621	-0.256326	-0.917086
O	4.847572	0.858966	-1.721345
P	5.789484	1.577778	-2.784268
O	6.984715	0.754435	-3.087353
N	-0.184353	-3.394308	4.104090
O	4.870864	1.946999	-3.908973
O	6.278113	2.897527	-2.038129
P	5.823876	4.448014	-1.974217
O	6.846183	5.111237	-1.112622
O	5.644011	4.967985	-3.356215
O	4.471795	4.388940	-1.167305
P	2.848690	4.363266	-1.480705
O	2.273622	3.883838	-0.170176
O	2.473143	5.777729	-1.840163
O	2.660675	3.386401	-2.615988
O	4.226696	4.755847	-5.816853
O	6.428076	4.179170	-7.531633
O	5.797239	7.788283	-3.992978
O	9.037713	0.648255	-0.981255
O	5.813876	-1.040892	-5.171126
O	5.609770	1.480859	-6.719840
O	9.141228	2.015070	-4.648081
O	9.046779	3.412046	0.024391
O	9.244509	6.024718	-2.708953
O	6.329650	8.091998	-1.109363

O	6.278299	5.336834	1.747569
O	2.947777	1.272365	-7.804559
O	3.140877	-0.194173	-4.501277
O	7.966584	4.676847	-5.088271
Mg	2.867314	1.752391	-3.688918
H	3.051403	-4.630130	1.488144
H	-0.714854	-2.639517	4.481100
H	-0.697209	-4.207287	3.839005
H	2.393032	1.084118	4.242168
H	4.427132	1.141974	3.064286
H	5.644278	-1.392764	3.429316
H	7.512979	0.142518	3.136512
H	5.755873	-1.890504	1.106083
H	7.915831	-1.752578	1.281506
H	6.063134	1.067817	0.540104
H	6.104656	-0.719004	-1.327820
H	4.401396	-0.958707	-0.960809
H	6.342901	-0.625570	-4.491640
H	5.404007	1.741385	-5.822270
H	8.465148	1.553130	-4.156892
H	8.420425	0.650216	-1.711753
H	5.773822	6.843921	-3.838579
H	7.174615	4.740860	-4.553539
H	5.625908	4.489096	-7.106086
H	4.628638	4.723901	-4.946163
H	6.574670	7.170756	-1.046940
H	6.465825	5.258845	0.812505
H	8.320828	3.889258	-0.370453
H	8.508768	5.763186	-2.159212
H	1.707619	6.362084	-3.443250
H	0.730087	6.483577	-1.214766
H	3.865125	7.650362	1.361416
H	3.124921	7.258201	-0.976322
H	3.871636	1.252867	-7.546872
H	4.009729	-0.547629	-4.711939
H	1.825137	2.132131	0.000714
H	3.342771	3.390641	5.372239
H	3.065684	4.255242	1.474931
H	0.630110	4.277967	0.628412
H	-0.686783	4.208028	-5.020045
H	3.757463	6.661855	-6.012344
H	5.931473	-0.487630	-5.938829
H	8.613946	0.147937	-0.288697
H	6.010330	2.247528	-7.125850
H	8.803038	2.900373	-4.771067
H	2.622088	-0.902624	-4.136851
H	2.692880	0.368674	-7.950677
H	3.547236	4.088126	-5.810015
H	6.464123	4.590023	-8.387786
H	7.656990	4.587318	-5.987826
H	5.989805	8.155332	-3.132621
H	5.407970	8.126914	-0.856794
H	5.511906	4.790034	1.902835
H	9.016749	2.527743	-0.336788
H	9.045734	5.676645	-3.573110
O	-0.110281	6.781431	-0.867759

H	-0.332542	6.139911	-0.196873
O	4.153383	7.361749	2.226547
H	5.013855	6.971798	2.087350
O	3.482357	8.026677	-0.515964
H	2.942277	8.768045	-0.763970
O	1.272554	6.691656	-4.233959
H	1.965647	7.068193	-4.774832
O	3.463097	4.497936	2.316446
H	3.425215	5.451950	2.355871
O	2.579862	3.373276	4.807144
H	2.868759	3.734246	3.967829
O	1.598700	1.196017	0.029647
H	2.375341	0.766625	0.377667
O	-0.205282	4.547645	1.019815
H	-0.825788	3.856791	0.819887
O	0.106611	4.426524	-5.495140
H	0.468923	5.208172	-5.067267
O	3.542788	7.578891	-5.845920
H	4.210357	7.871481	-5.227066
O	2.129293	2.516227	-5.431968
H	2.226428	2.064690	-6.276298
H	1.378198	3.119680	-5.480290
O	1.302677	0.762907	-2.684577
H	0.413279	0.975813	-2.949080
H	1.338145	0.870184	-1.723505

[Mg-ATP]²⁻ (Mg²⁺ bound to β- and γ-phosphate)

C	7.224927	-0.822676	1.178578
C	6.400689	0.390773	1.648327
O	5.741657	0.889906	0.512408
C	6.357295	0.400165	-0.665258
C	6.764706	-1.015146	-0.271981
N	5.429865	0.126595	2.680502
C	4.426729	-0.802826	2.709145
C	3.760179	-0.587106	3.893105
N	4.331220	0.463841	4.589294
C	5.297970	0.850033	3.838275
N	4.132054	-1.736044	1.805532
C	3.098102	-2.463627	2.163904
N	2.364894	-2.366194	3.267622
C	2.673168	-1.429240	4.163609
N	1.957320	-1.353158	5.298273
C	5.383016	0.475700	-1.817277
O	5.034723	1.825785	-2.085047
P	5.533519	2.671333	-3.330859
O	7.086128	2.959546	-2.998166
P	7.796586	4.068300	-2.077932
O	9.114600	3.311294	-1.667383
P	10.678216	3.215316	-2.178902
O	10.922827	4.458632	-3.017769
O	7.777934	-1.506934	-1.105013
O	8.578676	-0.448645	1.231810
O	4.774182	3.950285	-3.325847
O	5.528548	1.824879	-4.556795
O	8.111996	5.247946	-2.943544
O	6.986746	4.312065	-0.857579

O	11.454269	3.203851	-0.883496
O	10.774878	1.951695	-2.989088
O	7.892952	3.910242	1.866903
O	8.886263	6.585860	1.873713
O	4.444713	3.630963	0.526843
O	6.631657	7.046811	-0.114316
O	2.995563	0.236236	-4.751444
O	7.395943	-1.171897	-7.894599
O	7.824774	0.477340	-5.580742
O	4.831772	2.698903	-7.194269
O	2.431757	3.795051	-1.615895
O	4.636346	6.771471	-2.335407
O	1.385435	1.259172	-2.503023
O	4.035588	5.163317	-5.855433
O	12.966150	4.476538	-5.001197
O	14.234390	4.236107	-1.054033
O	13.102625	0.908295	-0.257338
O	10.128784	2.142256	1.496512
O	11.223501	5.922243	0.264295
O	13.307154	0.620968	-3.152611
O	9.350816	-0.462957	-3.353000
O	10.034819	2.394841	-5.715182
O	15.023858	2.932689	-3.590595
O	10.321438	7.235626	-2.025491
O	6.733315	6.081292	-5.374094
O	9.472906	5.150173	-5.608173
Mg	9.851872	6.021003	-3.696028
H	2.801346	-3.237732	1.480314
H	2.035870	-0.538121	5.866455
H	1.088072	-1.840026	5.337770
H	5.967154	1.657172	4.057903
H	7.068832	1.137048	2.046875
H	7.057422	-1.696537	1.791669
H	9.083442	-1.045094	0.688867
H	5.903130	-1.666458	-0.293672
H	7.705345	-2.449706	-1.196279
H	7.241875	0.986102	-0.886453
H	5.815846	0.010135	-2.691753
H	4.465763	-0.036247	-1.564339
H	0.468714	1.380529	-2.720858
H	3.103148	3.902189	-2.288935
H	4.740231	5.856743	-2.593883
H	4.110315	4.771779	-4.985102
H	3.820253	0.716911	-4.739126
H	5.122023	2.366727	-6.342873
H	7.053876	0.926309	-5.228815
H	6.666984	-1.751152	-7.707936
H	6.785323	6.124739	-0.322195
H	5.173605	3.989064	0.023919
H	7.563655	3.969013	0.970381
H	8.535770	5.702781	2.004410
H	13.327405	3.942895	-0.983119
H	11.243794	4.997076	0.018199
H	10.514336	2.459124	0.678530
H	12.526669	1.657321	-0.424827
H	14.536007	2.115559	-3.482834

H	12.451211	1.046945	-3.232718
H	9.814979	0.346478	-3.128514
H	10.344013	2.228645	-4.821276
H	10.657318	6.801758	-1.232143
H	12.299761	4.271847	-4.340567
H	6.796653	5.660194	-4.519793
H	8.570916	5.300176	-5.884832
H	2.481603	0.582441	-4.023542
H	7.518432	-0.640673	-7.106659
H	5.614821	2.787914	-7.724618
H	8.259211	0.066565	-4.830605
H	4.197890	4.439183	-6.458247
H	4.757724	7.277308	-3.130167
H	2.937496	3.704587	-0.808888
H	1.692518	2.102843	-2.164560
H	4.659113	2.704974	0.598189
H	8.656785	3.335200	1.816173
H	8.258972	7.017199	1.299901
H	5.957097	7.303932	-0.737174
H	10.476687	6.050143	0.849382
H	9.690837	1.319313	1.296189
H	12.578179	0.273310	0.215853
H	14.571194	3.829778	-1.850518
H	13.410962	0.503367	-2.210164
H	14.479139	3.473358	-4.159442
H	8.845222	-0.714022	-2.584581
H	9.265208	1.836569	-5.818751
H	9.666441	7.863729	-1.741839
H	12.703440	4.018541	-5.791878
H	5.841635	5.917281	-5.682034
H	9.630392	4.202328	-5.678875
O	11.583857	6.941532	-4.587323
H	12.055758	7.491578	-3.970534
H	12.216189	6.299676	-4.913845
O	8.753769	7.733178	-4.382556
H	9.228149	8.347153	-4.933370
H	7.950080	7.504803	-4.851660

Mg₂ATP

C	4.804353	-2.044697	2.701936
C	3.876445	-0.891776	2.280688
O	4.622018	-0.061753	1.423674
C	6.001809	-0.379617	1.484242
C	6.021542	-1.875544	1.783454
N	2.652832	-1.277726	1.621047
C	2.474243	-2.055614	0.510115
C	1.117379	-2.065474	0.282912
N	0.458978	-1.302476	1.231278
C	1.398245	-0.861098	1.986650
N	3.392489	-2.690404	-0.216019
C	2.860173	-3.355109	-1.216816
N	1.578346	-3.451237	-1.552825
C	0.670651	-2.813736	-0.814591
N	-0.629742	-2.942833	-1.127521
C	6.675508	-0.022183	0.180986
O	6.796909	1.399933	0.080616

P	6.235297	2.312314	-1.077266
O	7.571068	2.721022	-1.885626
P	8.433327	4.029580	-2.127009
O	9.887806	3.521138	-1.875696
P	11.321475	3.653127	-2.723855
O	11.112631	4.887803	-3.595123
O	7.223982	-2.236468	2.400910
O	5.150003	-1.820654	4.041949
O	5.709644	3.555181	-0.415827
O	5.342659	1.580368	-1.995899
O	8.246764	4.470205	-3.546439
O	8.077043	5.063826	-1.093594
O	12.356882	3.840869	-1.661488
O	11.433976	2.378364	-3.517332
O	9.713503	5.174158	1.404418
O	12.230864	7.350195	-2.251523
O	15.112046	3.708783	-2.466214
O	13.328584	1.659443	-0.057317
O	12.470492	5.863210	0.323821
O	5.642065	-1.003469	-3.450953
O	8.413788	-0.724556	-4.227877
O	2.624781	2.740919	-1.830359
O	5.062460	2.206651	-4.935351
O	3.340549	5.402558	-2.623285
O	3.268873	2.671399	1.078026
O	14.045374	0.981916	-2.870891
O	10.375003	-0.069331	-2.231987
O	13.088559	2.674845	-5.957276
O	9.619907	1.628424	-5.636770
O	8.557662	8.028516	-2.204608
O	5.459659	5.086721	-4.657410
O	9.533903	4.335150	-6.458750
O	9.249968	7.291647	-4.765676
O	11.976710	4.533614	-7.783921
Mg	9.587825	5.319249	-4.716460
Mg	6.399835	5.338064	-0.096349
O	5.042777	6.616770	-0.780055
O	7.032802	5.851096	1.734625
H	3.543754	-3.891299	-1.849023
H	-1.289395	-2.313371	-0.725203
H	-0.861864	-3.318085	-2.021692
H	1.259320	-0.225029	2.837334
H	3.582662	-0.341848	3.161135
H	4.329922	-3.010147	2.592997
H	5.990478	-2.232022	4.213933
H	5.869249	-2.439883	0.874818
H	7.465607	-3.122978	2.162373
H	6.466972	0.161944	2.300684
H	7.675730	-0.428620	0.164149
H	6.112873	-0.405042	-0.654313
H	14.211303	3.891632	-2.192413
H	12.313867	7.044711	-1.351113
H	12.467881	5.120780	-0.283507
H	12.965685	2.442298	-0.474499
H	10.213543	1.828022	-4.907365
H	12.564175	2.599979	-5.159284

H	13.178979	1.312016	-3.101922
H	10.732207	0.736986	-2.601656
H	3.437697	2.277367	-2.025101
H	5.170884	1.976561	-4.016429
H	8.620939	0.023945	-4.782392
H	5.471818	-0.206892	-2.955973
H	4.028637	3.174520	0.798353
H	3.038883	4.528262	-2.358127
H	9.487713	5.192485	0.477869
H	8.529655	7.184312	-1.763699
H	8.955037	7.691732	-3.933781
H	12.446954	3.895501	-7.239905
H	6.307144	5.015089	-4.227297
H	9.440902	3.384160	-6.328654
H	6.552660	-0.929552	-3.735458
H	8.989790	-0.628177	-3.469743
H	2.572828	2.726203	-0.876651
H	5.162073	3.156136	-4.966635
H	10.462553	0.009721	-1.282196
H	14.604890	1.755583	-2.881667
H	10.141847	1.149180	-6.271569
H	13.988965	2.777371	-5.671468
H	11.684828	5.755331	0.852784
H	11.896260	6.599747	-2.737010
H	13.694439	1.167224	-0.788328
H	15.306488	4.320078	-3.166784
H	8.822555	7.747197	-5.484681
H	12.066454	4.244227	-8.685332
H	9.683682	4.246291	1.639857
H	7.708403	8.437288	-2.042735
H	3.606477	1.790550	1.217718
H	2.575596	5.867931	-2.943690
H	4.816272	5.247538	-3.969252
H	10.296580	4.452803	-7.038427
H	5.273276	7.512535	-1.046483
H	4.390073	6.276122	-1.404727
H	6.696727	6.567479	2.265073
H	7.978734	5.761306	1.899928
O	5.930027	9.173328	-1.580384
O	12.771620	7.289343	-7.199866
H	13.467870	7.260605	-6.554727
H	12.555961	6.378697	-7.393429
H	5.959206	9.830981	-0.892722
H	5.463091	9.575138	-2.306195
H	8.347178	2.152908	1.353137
O	9.155302	2.323084	1.830587
H	8.973963	2.096378	2.736471
H	10.342063	0.926161	1.027361
O	10.902707	0.275293	0.610465
H	11.746330	0.708590	0.473458

Mg-ADP⁻

C	-5.727742	-2.073887	1.617346
C	-5.224173	-0.847915	2.073160
C	-3.876909	-0.631798	1.896894

N	-3.016721	-1.479160	1.334261
C	-3.598978	-2.591996	0.947199
N	-4.878976	-2.931823	1.052421
N	-5.814779	0.239375	2.692804
C	-4.846308	1.062750	2.872635
N	-3.633790	0.606724	2.423419
C	-2.398543	1.350543	2.474325
O	-2.010089	1.691152	1.168649
C	-0.609985	1.548361	0.998441
C	-0.243573	0.406305	1.939616
C	-1.206082	0.618738	3.116842
O	-0.664460	1.490885	4.070920
O	1.105361	0.481168	2.315691
C	-0.317268	1.278175	-0.457548
O	-0.732403	2.412986	-1.194019
P	-0.792454	2.451343	-2.787461
O	0.721488	2.585087	-3.244411
P	1.815139	3.827202	-3.145187
O	2.562101	3.618876	-1.859478
N	-7.015103	-2.431326	1.759827
O	-1.305224	1.160342	-3.319535
O	-1.550783	3.695474	-3.123086
Mg	-0.932277	5.604549	-3.398920
O	-0.834704	5.411240	-5.522421
O	2.652811	3.639048	-4.392242
O	0.986312	5.093620	-3.176283
O	-2.935261	6.331387	-3.758045
O	-1.333555	6.005480	-1.337051
O	2.974333	1.116462	-5.571482
O	1.822089	5.287023	-6.505766
O	-3.082198	4.305478	0.130031
O	-1.575569	0.602299	-6.088784
O	2.262469	4.856680	0.669446
O	5.387176	3.420986	-1.693213
O	0.886826	1.083143	-7.554150
O	1.365529	3.609508	-8.804159
O	2.937550	2.761254	2.641401
O	1.830780	7.957636	-5.380714
O	5.410157	4.185569	-4.553409
H	-2.964359	-3.324531	0.483245
H	-7.690875	-1.732284	1.978716
H	-7.342371	-3.220232	1.245308
H	-4.932558	2.026979	3.330946
H	-2.607391	2.243619	3.042705
H	-1.501858	-0.310888	3.582916
H	0.225162	1.220208	4.269619
H	-0.452987	-0.543973	1.471042
H	1.466462	-0.387893	2.444381
H	-0.112602	2.459946	1.310587
H	0.745258	1.116502	-0.590825
H	-0.858241	0.404355	-0.792564
H	0.063304	0.948062	-7.084748
H	1.579346	1.039109	-6.893777
H	3.848566	1.100179	-5.942343
H	2.878904	1.974455	-5.143496
H	-3.226296	6.434420	-4.664989

H	-3.643079	5.904199	-3.287566
H	-1.489096	6.894436	-1.038894
H	-1.924410	5.432999	-0.839757
H	-1.485736	0.792121	-5.150847
H	-1.834734	-0.309723	-6.148185
H	0.034192	5.413381	-5.930931
H	-1.443654	5.856499	-6.107496
H	2.147652	4.696589	-5.816533
H	1.759576	4.768175	-7.308811
H	2.661166	8.121305	-4.948353
H	1.925309	7.115143	-5.825646
H	5.787328	3.545866	-5.145463
H	4.463635	4.010942	-4.537550
H	5.628073	3.657913	-2.585416
H	4.427518	3.463099	-1.688997
H	2.329955	2.029760	2.551140
H	2.812203	3.096705	3.521531
H	2.072884	3.469590	-9.422863
H	1.168509	2.749229	-8.425246
H	2.483685	4.169770	1.294233
H	-3.437200	4.662849	0.935819
H	-2.696640	3.463287	0.363982
H	2.326216	4.455964	-0.200859
O	-0.329561	7.655164	-3.551831
H	0.414535	7.800801	-4.144194
H	-0.995957	8.289667	-3.792203
H	-2.879153	0.258163	-2.774953
O	-3.674661	-0.220093	-2.532703
H	-3.615523	-0.361552	-1.595523
O	-3.203709	6.676603	-6.587334
H	-3.800074	6.159670	-7.119010
H	-3.249495	7.563521	-6.929016

Cartesian coordinates of the structures used to calculate Mg 2s and 2p binding energies

Mg²⁺

O	0.072366	-0.129916	2.107291
Mg	0.049674	-0.070827	0.021061
O	-0.082109	2.010599	0.045619
O	2.131537	0.080743	0.051556
O	0.233170	-2.150329	-0.005718
O	-2.031702	-0.227752	-0.001682
O	0.040450	-0.005867	-2.065630
H	-0.269093	2.540703	-0.723031
H	-0.279267	2.540271	0.811921
H	0.808019	-0.130612	-2.615352
H	-0.722817	-0.220704	-2.593172
H	2.711156	-0.649261	-0.143647
H	2.606099	0.881248	-0.150692
H	0.059248	-2.699291	-0.764218
H	0.113647	-2.692311	0.768282
H	-2.522851	-1.023647	0.177885
H	-2.626266	0.505802	0.121865
H	0.844281	0.082329	2.623122
H	-0.687708	0.015317	2.662378

[Mg-ATP]²⁻

C	0.954635	-3.123957	3.443092
C	1.610854	-1.889433	3.533673
C	2.789449	-1.766177	2.834651
N	3.356160	-2.711252	2.086101
C	2.654092	-3.822032	2.074538
N	1.508199	-4.078531	2.695855
N	1.315758	-0.714236	4.201936
C	2.287604	0.072025	3.904475
N	3.229610	-0.495530	3.083724
C	4.391895	0.185018	2.568644
O	4.242835	0.366270	1.182247
C	5.473575	0.158313	0.513960
C	6.155354	-0.917085	1.351917
C	5.737815	-0.535146	2.777581
O	6.619309	0.403858	3.330351
O	7.543763	-0.887231	1.156396
C	5.220621	-0.256326	-0.917086
O	4.847572	0.858966	-1.721345
P	5.789484	1.577778	-2.784268
O	6.984715	0.754435	-3.087353
N	-0.184353	-3.394308	4.104090
O	4.870864	1.946999	-3.908973
O	6.278113	2.897527	-2.038129
P	5.823876	4.448014	-1.974217
O	6.846183	5.111237	-1.112622
O	5.644011	4.967985	-3.356215
O	4.471795	4.388940	-1.167305
P	2.848690	4.363266	-1.480705
O	2.273622	3.883838	-0.170176
O	2.473143	5.777729	-1.840163
O	2.660675	3.386401	-2.615988
O	4.226696	4.755847	-5.816853

O	6.428076	4.179170	-7.531633
O	5.797239	7.788283	-3.992978
O	9.037713	0.648255	-0.981255
O	5.813876	-1.040892	-5.171126
O	5.609770	1.480859	-6.719840
O	9.141228	2.015070	-4.648081
O	9.046779	3.412046	0.024391
O	9.244509	6.024718	-2.708953
O	6.329650	8.091998	-1.109363
O	6.278299	5.336834	1.747569
O	2.947777	1.272365	-7.804559
O	3.140877	-0.194173	-4.501277
O	7.966584	4.676847	-5.088271
Mg	2.867314	1.752391	-3.688918
H	3.051403	-4.630130	1.488144
H	-0.714854	-2.639517	4.481100
H	-0.697209	-4.207287	3.839005
H	2.393032	1.084118	4.242168
H	4.427132	1.141974	3.064286
H	5.644278	-1.392764	3.429316
H	7.512979	0.142518	3.136512
H	5.755873	-1.890504	1.106083
H	7.915831	-1.752578	1.281506
H	6.063134	1.067817	0.540104
H	6.104656	-0.719004	-1.327820
H	4.401396	-0.958707	-0.960809
H	6.342901	-0.625570	-4.491640
H	5.404007	1.741385	-5.822270
H	8.465148	1.553130	-4.156892
H	8.420425	0.650216	-1.711753
H	5.773822	6.843921	-3.838579
H	7.174615	4.740860	-4.553539
H	5.625908	4.489096	-7.106086
H	4.628638	4.723901	-4.946163
H	6.574670	7.170756	-1.046940
H	6.465825	5.258845	0.812505
H	8.320828	3.889258	-0.370453
H	8.508768	5.763186	-2.159212
H	1.707619	6.362084	-3.443250
H	0.730087	6.483577	-1.214766
H	3.865125	7.650362	1.361416
H	3.124921	7.258201	-0.976322
H	3.871636	1.252867	-7.546872
H	4.009729	-0.547629	-4.711939
H	1.825137	2.132131	0.000714
H	3.342771	3.390641	5.372239
H	3.065684	4.255242	1.474931
H	0.630110	4.277967	0.628412
H	-0.686783	4.208028	-5.020045
H	3.757463	6.661855	-6.012344
H	5.931473	-0.487630	-5.938829
H	8.613946	0.147937	-0.288697
H	6.010330	2.247528	-7.125850
H	8.803038	2.900373	-4.771067
H	2.622088	-0.902624	-4.136851
H	2.692880	0.368674	-7.950677

H	3.547236	4.088126	-5.810015
H	6.464123	4.590023	-8.387786
H	7.656990	4.587318	-5.987826
H	5.989805	8.155332	-3.132621
H	5.407970	8.126914	-0.856794
H	5.511906	4.790034	1.902835
H	9.016749	2.527743	-0.336788
H	9.045734	5.676645	-3.573110
O	-0.110281	6.781431	-0.867759
H	-0.332542	6.139911	-0.196873
O	4.153383	7.361749	2.226547
H	5.013855	6.971798	2.087350
O	3.482357	8.026677	-0.515964
H	2.942277	8.768045	-0.763970
O	1.272554	6.691656	-4.233959
H	1.965647	7.068193	-4.774832
O	3.463097	4.497936	2.316446
H	3.425215	5.451950	2.355871
O	2.579862	3.373276	4.807144
H	2.868759	3.734246	3.967829
O	1.598700	1.196017	0.029647
H	2.375341	0.766625	0.377667
O	-0.205282	4.547645	1.019815
H	-0.825788	3.856791	0.819887
O	0.106611	4.426524	-5.495140
H	0.468923	5.208172	-5.067267
O	3.542788	7.578891	-5.845920
H	4.210357	7.871481	-5.227066
O	2.129293	2.516227	-5.431968
H	2.226428	2.064690	-6.276298
H	1.378198	3.119680	-5.480290
O	1.302677	0.762907	-2.684577
H	0.413279	0.975813	-2.949080
H	1.338145	0.870184	-1.723505

Mg₂ATP

C	4.804353	-2.044697	2.701936
C	3.876445	-0.891776	2.280688
O	4.622018	-0.061753	1.423674
C	6.001809	-0.379617	1.484242
C	6.021542	-1.875544	1.783454
N	2.652832	-1.277726	1.621047
C	2.474243	-2.055614	0.510115
C	1.117379	-2.065474	0.282912
N	0.458978	-1.302476	1.231278
C	1.398245	-0.861098	1.986650
N	3.392489	-2.690404	-0.216019
C	2.860173	-3.355109	-1.216816
N	1.578346	-3.451237	-1.552825
C	0.670651	-2.813736	-0.814591
N	-0.629742	-2.942833	-1.127521
C	6.675508	-0.022183	0.180986
O	6.796909	1.399933	0.080616
P	6.235297	2.312314	-1.077266
O	7.571068	2.721022	-1.885626
P	8.433327	4.029580	-2.127009

O	9.887806	3.521138	-1.875696
P	11.321475	3.653127	-2.723855
O	11.112631	4.887803	-3.595123
O	7.223982	-2.236468	2.400910
O	5.150003	-1.820654	4.041949
O	5.709644	3.555181	-0.415827
O	5.342659	1.580368	-1.995899
O	8.246764	4.470205	-3.546439
O	8.077043	5.063826	-1.093594
O	12.356882	3.840869	-1.661488
O	11.433976	2.378364	-3.517332
O	9.713503	5.174158	1.404418
O	12.230864	7.350195	-2.251523
O	15.112046	3.708783	-2.466214
O	13.328584	1.659443	-0.057317
O	12.470492	5.863210	0.323821
O	5.642065	-1.003469	-3.450953
O	8.413788	-0.724556	-4.227877
O	2.624781	2.740919	-1.830359
O	5.062460	2.206651	-4.935351
O	3.340549	5.402558	-2.623285
O	3.268873	2.671399	1.078026
O	14.045374	0.981916	-2.870891
O	10.375003	-0.069331	-2.231987
O	13.088559	2.674845	-5.957276
O	9.619907	1.628424	-5.636770
O	8.557662	8.028516	-2.204608
O	5.459659	5.086721	-4.657410
O	9.533903	4.335150	-6.458750
O	9.249968	7.291647	-4.765676
O	11.976710	4.533614	-7.783921
Mg	9.587825	5.319249	-4.716460
Mg	6.399835	5.338064	-0.096349
O	5.042777	6.616770	-0.780055
O	7.032802	5.851096	1.734625
H	3.543754	-3.891299	-1.849023
H	-1.289395	-2.313371	-0.725203
H	-0.861864	-3.318085	-2.021692
H	1.259320	-0.225029	2.837334
H	3.582662	-0.341848	3.161135
H	4.329922	-3.010147	2.592997
H	5.990478	-2.232022	4.213933
H	5.869249	-2.439883	0.874818
H	7.465607	-3.122978	2.162373
H	6.466972	0.161944	2.300684
H	7.675730	-0.428620	0.164149
H	6.112873	-0.405042	-0.654313
H	14.211303	3.891632	-2.192413
H	12.313867	7.044711	-1.351113
H	12.467881	5.120780	-0.283507
H	12.965685	2.442298	-0.474499
H	10.213543	1.828022	-4.907365
H	12.564175	2.599979	-5.159284
H	13.178979	1.312016	-3.101922
H	10.732207	0.736986	-2.601656
H	3.437697	2.277367	-2.025101

H	5.170884	1.976561	-4.016429
H	8.620939	0.023945	-4.782392
H	5.471818	-0.206892	-2.955973
H	4.028637	3.174520	0.798353
H	3.038883	4.528262	-2.358127
H	9.487713	5.192485	0.477869
H	8.529655	7.184312	-1.763699
H	8.955037	7.691732	-3.933781
H	12.446954	3.895501	-7.239905
H	6.307144	5.015089	-4.227297
H	9.440902	3.384160	-6.328654
H	6.552660	-0.929552	-3.735458
H	8.989790	-0.628177	-3.469743
H	2.572828	2.726203	-0.876651
H	5.162073	3.156136	-4.966635
H	10.462553	0.009721	-1.282196
H	14.604890	1.755583	-2.881667
H	10.141847	1.149180	-6.271569
H	13.988965	2.777371	-5.671468
H	11.684828	5.755331	0.852784
H	11.896260	6.599747	-2.737010
H	13.694439	1.167224	-0.788328
H	15.306488	4.320078	-3.166784
H	8.822555	7.747197	-5.484681
H	12.066454	4.244227	-8.685332
H	9.683682	4.246291	1.639857
H	7.708403	8.437288	-2.042735
H	3.606477	1.790550	1.217718
H	2.575596	5.867931	-2.943690
H	4.816272	5.247538	-3.969252
H	10.296580	4.452803	-7.038427
H	5.273276	7.512535	-1.046483
H	4.390073	6.276122	-1.404727
H	6.696727	6.567479	2.265073
H	7.978734	5.761306	1.899928
O	5.930027	9.173328	-1.580384
O	12.771620	7.289343	-7.199866
H	13.467870	7.260605	-6.554727
H	12.555961	6.378697	-7.393429
H	5.959206	9.830981	-0.892722
H	5.463091	9.575138	-2.306195
H	8.347178	2.152908	1.353137
O	9.155302	2.323084	1.830587
H	8.973963	2.096378	2.736471
H	10.342063	0.926161	1.027361
O	10.902707	0.275293	0.610465
H	11.746330	0.708590	0.473458

References

1. ACD/ChemSketch. Advanced Chemistry Development, Inc. (ACD Labs): Toronto, ON, Canada.
2. Storer, A.C. and A. Cornish-Bowden, *Concentration of MgATP²⁻ and other ions in solution. Calculation of the true concentrations of species present in mixtures of associating ions.* Biochem J, 1976. **159**(1): p. 1-5.
3. *Maple 2016.* Maplesoft, a division of Waterloo Maple Inc.: Waterloo, Ontario.
4. Winter, B., et al., *Full Valence Band Photoemission from Liquid Water Using EUV Synchrotron Radiation.* The Journal of Physical Chemistry A, 2004. **108**(14): p. 2625-2632.
5. Weber, R., et al., *Photoemission from Aqueous Alkali-Metal-Iodide Salt Solutions Using EUV Synchrotron Radiation.* The Journal of Physical Chemistry, 2004. **108**: p. 4729-4736.
6. Schroeder, C., *Quantifying Aspects of DNA Damage. Ph.D. dissertation.* University of Southern California: Los Angeles, CA USA
7. Schroeder, C.A., et al., *Oxidation Half-Reaction of Aqueous Nucleosides and Nucleotides via Photoelectron Spectroscopy Augmented by ab Initio Calculations.* Journal of the American Chemical Society, 2015. **137**(1): p. 201-209.
8. Frańska, M., et al., *Gas-Phase Internal Ribose Residue Loss from Mg-ATP and Mg-ADP Complexes: Experimental and Theoretical Evidence for Phosphate-Mg-Adenine Interaction.* Journal of the American Society for Mass Spectrometry, 2022. **33**(8): p. 1474-1479.